NATIONAL ADVISORY COMMITTEE FOR AERONAUTICS

ADVANCE CONFIDENTIAL REPORT

EFFECTS OF DIRECTION OF PROPELLER ROTATION ON THE LONGITUDINAL STABILITY OF THE 1/10-SCALE MODEL OF THE NORTH AMERICAN XB-28 AIRPLANE WITH FLAPS NEUTRAL

By Noel K. Delany
Ames Aeronautical Laboratory

June 1942

NATIONAL ADVISORY COMMITTEE FOR AERONAUTICS

ADVANCE CONFIDENTIAL REPORT

EFFECTS OF DIRECTION OF PROPELLER ROTATION ON THE LONGITUDINAL STABILITY OF THE 1/10-SCALE MODEL OF THE NORTH AMERICAN XB-28 AIRPLANE WITH FLAPS NEUTRAL

By Noel K. Delany

SUMMARY

The effects of direction of propeller rotation on factors affecting the longitudinal stability of the XB-28 airplane were measured on a 1/10-scale model in the 7- by 10-foot tunnel of the Ames Aeronautical Laboratory. The main effect observed was that caused by regions of high downwash behind the nacelles (power off as well as power on with flaps neutral). The optimum direction of propeller rotation, both propellers rotating up toward the fuselage, shifted this region off the horizontal tail and thus removed its destabilizing effect. Rotating both propellers downward toward the fuselage moved it inboard on the tail and accentuated the effect, while rotating both propellers right hand had an intermediate result.

Comparisons are made of the tail effects as measured by force tests with those predicted from the point-by-point downwash and velocity surveys in the region of the tail. These surveys in turn are compared with the results predicted from available theory.

INTRODUCTION

At the request of the Bureau of Aeronautics, Navy Department, tests were conducted on a 1/10-scale model of the XB-28 airplane in the 7- by 10-foot tunnel 2 to determine the effect of mode of propeller rotation on the longitudinal stability characteristics. The results of reference 1 showed the marked effect which the mode of propeller rotation has on the longitudinal stability characteristics of the XB-28. The purpose of the tests reported herein was to measure the changes in downwash and velocity distribution in the region of the horizontal

tail surface associated with the various modes of propeller rotation, thereby establishing a basis for the change in the longitudinal stability characteristics.

MODEL AND APPARATUS

The 1/10-scale model of the North American XB-28 airplane was furnished by North American Aviation Inc. Figure 1 is a three-view drawing of the model, and figure 2 shows the model as it was mounted in the tunnel.

The model dimensions were as follows:

S wing area (6.759 sq ft)

c mean aerodynamic chord (1.001 ft)

b wing span (7.261 ft)

D propeller diameter (1.388 ft)

The model configuration was maintained throughout the tests as shown in figure 1 except that the horizontal tail, which had a dihedral angle of 7.5°, was removed for surveys and for "tail off" force tests.

Three four-blade, 1.388-feet-diameter propellers were furnished with the model. Two were right-hand propellers and one left-hand. The propellers were set at a blade angle of 40.5° at the 0.75R station throughout the tests.

A calibrated 0.25-inch diameter directional pitot tube was for the point-by-point surveys. The tube was mounted on a strut which enabled it to be moved vertically, longitudinally, and laterally from outside of the test section.

COEFFICIENTS AND SYMBOLS

The results of the tests are given in the form of standard NACA coefficients of forces and moments based on model wing area, wing span, and mean aerodynamic chord. All moments are given about the center-of-gravity location on the fuselage reference line at 26 percent of the

mean aerodynamic chord. The data are referred to the wind axes. Since all the tests were conducted at zero yaw, the wind axes correspond with the body axes.

The coefficients and symbols used in this report are as follows:

Coefficients

C_{D_R} resultant drag coefficient, $\frac{D}{qS}$

C_L lift coefficient, $\frac{L}{qS}$

C_m pitching-moment coefficient, $\frac{M}{qSc}$

C_{m_t} pitching-moment coefficient due to the horizontal tail, $\frac{M_t}{qSc}$

where

D force along X axis; positive when directed backward

L force along Z axis; positive when directed upward

M pitching moment about Y axis; positive when it tends to raise the nose

M_t pitching-moment horizontal tail on less pitching-moment horizontal tail off

q dynamic pressure, $\frac{1}{2}\rho V^2$

S wing area (6.759 ft)

c mean aerodynamic chord (1.001 ft)

The following propeller coefficients were used:

T_c propulsive thrust coefficient, $\frac{T}{\rho V^2 D^2}$

T_c' effective thrust coefficient, $\frac{T_e}{\rho V^2 D^2}$

$\frac{V}{nD}$ advance diameter ratio

T propulsive thrust of one propeller and nacelle combination

T_e effective thrust, $T-\Delta D$

ΔD increment of drag due to increased velocity in slipstream of propeller

ρ mass density of air in slugs per cubic foot

V airspeed in feet per second

D propeller diameter (1.388 ft)

n propeller rotational speed in revolutions per second

Symbols

α angle of attack of fuselage reference line, degrees

α_u uncorrected angle of attack of fuselage reference line, degrees

α_t resultant aerodynamic angle of attack of the horizontal tail ($\alpha_t = \alpha + i_t - \epsilon$)

i_t angle of stabilizer setting with respect to fuselage reference line, degrees (positive with trailing edge down)

ϵ downwash angle measured from the longitudinal wind axis, degrees

$\frac{q}{q_o}$ ratio of local dynamic pressure to free-stream dynamic pressure

β propeller-blade angle setting at 75 percent radius

TARE AND TUNNEL-WALL CORRECTIONS

The lift, drag, pitching moment, and downwash have been corrected for tares caused by the struts. These tares were obtained from preliminary power-off tests, not presented in this report.

The angles of attack, drag coefficient, pitching-moment coefficient, and downwash angles have all been corrected for tunnel-wall effects. The jet-boundary corrections used were computed as follows and are all additive.

$$\Delta\alpha^{o} = \frac{\delta S C_L}{C} \times 57.3$$

$$\Delta\epsilon^{o} = \frac{\delta_2 S C_L}{C} \times 57.3$$

$$\Delta C_D = \frac{\delta S C_L^{\,2}}{C}$$

$$\Delta C_M = \left(\frac{\delta_1 S C_L}{C}\right)\left(\frac{dC_M}{di_t}\right) 57.3 \frac{q}{q_o}$$

where

$\delta = 0.114 \quad \delta_1 = 0.080 \quad \delta_2 = 0.194$

$\frac{dC_{m_t}}{di_t} = 0.030$ (from force tests)

$\frac{q}{q_o} = 1$ (assumed)

$S = 6.759$ square feet

$C = 70$ square feet

DESCRIPTION OF TESTS

The purpose of these tests was to measure the changes in downwash and velocity distribution in the region of the horizontal tail surface associated with various directions of propeller rotation. Two methods were used. The first method consisted of direct measurement of the stream angles and dynamic pressure with a calibrated pitch and yaw survey tube. A point-by-point survey was made across the tail span on a line corresponding approximately to the 25-percent chord line of the horizontal tail surface. The location of the survey line was 31.91 inches aft of the center of gravity (measured along the thrust axis) and 3.35 inches above the center of gravity (measured perpendicular to the thrust axis). Readings were taken starting $2\frac{1}{2}$ inches from the center line of the fuselage and progressing out in 1-inch increments. The set-up and apparatus used for these measurements are shown in figure 3.

The average downwash was also measured indirectly by

determining the angle of zero lift of the horizontal tail surfaces. For this purpose force tests were made with the horizontal tail surface incidence of 3.5°, 1.5°, 0°, −1.5°, −3.5°, −5.5°, and −7.5°. Figure 2 shows the model as mounted in the tunnel for force tests.

The tests outlined above were made power off and with propellers operating in the following directions.

1. 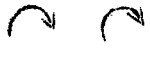 Both propellers rotating right hand

2.  Both propellers rotating up toward the fuselage

3.  Both propellers rotating down toward the fuselage

All propeller operating runs were made with a blade angle of 40.5°, at thrust conditions simulating steady flight at rated power (1625 hp, 1020 rpm at 25,000 ft) throughout the speed range. The computed thrust coefficient (T_c) versus C_L curve, which was matched in the running of the tests, is shown in figure 4. The computed T_c versus $\frac{V}{nD}$ for the model propeller at a blade angle of 40.5°, which was assumed, and the measured effective thrust coefficient (T_c') versus $\frac{V}{nD}$, are shown in figure 5.

RESULTS

The results are presented in figures 6 to 14. Figures 6 and 7 show the variation of lift and drag coefficient against α, for the various modes of propeller rotation, horizontal tail-off and horizontal tail-on $i_t = 1.5°$. Figures 8 to 11 present the following characteristics for the various directions of propeller rotation.

(a) Point-by-point downwash across horizontal tail span at approximately the 25-percent chord line

(b) Point by point q/q_o across the horizontal tail span at approximately the 25-percent chord line

(c) Effect of stabilizer setting on the pitching-moment coefficient

(d) Pitching-moment coefficient of the horizontal tail versus angle of incidence for various angles of attack

(e) Point-by-point tail effectiveness factor $\left(\frac{q}{q_o} c_{local} \alpha_t\right)$ across the horizontal tail span for an angle of incidence of the stabilizer of 1.5°.

The average downwash angles, as obtained from the point-by-point survey, are shown in figure 12. The average downwash from the angle of zero pitching-moment coefficient of the horizontal tail is shown in figure 13. Figure 14 shows the variation of average tail effectiveness factor for power off and the three directions of propeller rotation versus angle of attack.

DISCUSSION

Examination of the point-by-point power-off downwash survey (fig. 8(a)) shows regions of high downwash behind the nacelles at angles of attack above 5°. These regions have a marked destabilizing influence. They are probably caused by the "inwash" into the nacelle wake (treated quantitatively for two-dimensional wakes in reference 2) and the variation in lift over the span of the wing occupied by the nacelles. The major portion of the effects of propeller operation on stability can be traced to the shifting of these regions of downwash with various modes of propeller rotation.

With power off the outboard 22 percent of the horizontal tail is immersed in this region of high downwash. However, the longitudinal stability power off is satisfactory, the slope of the pitching-moment curve remaining approximately constant throughout the angle-of-attack range tested.

With both propellers rotating up toward the fuselage, both these regions are shifted outboard (since the tail plane is in the upper half of the slipstream) almost completely off the tail. The removal of the destabilizing

effects of this downwash region just about cancels the effects of the normal increase in downwash caused by the inclination of the thrust axis. As a result there is very little difference between the power off and the power on $\frac{dC_{m_t}}{dC_L}$ ($\frac{dC_{m_t}}{dC_L} = -0.211$ power on compared to $\frac{dC_{m_t}}{dC_L} = -0.253$ power off).

The opposite effect to that outlined above occurs with both propellers rotating down toward the fuselage. The regions of high downwash behind the nacelle are shifted inward to the larger chord portions of the tail (see fig. 11(a)), so that a larger tail area is affected. A secondary effect also occurs. At the higher angles and power conditions, the downwash behind the nacelle is high enough to cause a reversal in the angle of attack of the portion of the tail in this region, giving a downward (destabilizing) tail lift instead of an upward tail lift. This reverses the normal stabilizing effect of the increased velocity in the slipstream and causes it to have a destabilizing effect. This phenomenon is illustrated quantitatively in the plots of "tail effectiveness factor" versus tail span. The tail-effectiveness factor is taken as $\alpha_t \, c_{local} \, q/q_o$, the three factors of which tail lift is a function. The negative peaks (indicating negative lift, which is destabilizing in this case) which are evident on figure 11(e) are increased negatively by the higher velocity in slipstreams. All the effects outline above combine to decrease the average $\frac{dC_{m_t}}{dC_L}$ with both propellers rotating down toward the fuselage.

Both propellers rotating right hand gave stability intermediate between the two other modes of rotation. The destabilizing influences predominate, however; this is due in part to the reversal of the normally stabilizing effect of the increased velocity over a large portion of the tail in the slipstream. A $\frac{dC_{m_t}}{dC_L}$ of -0.184 results.

If considerations other than aerodynamic make it inadvisable to use the optimum mode of propeller rotation, both propellers rotating up toward the fuselage, two means of minimizing the unfavorable effects of both propellers rotating right hand suggest themselves. The first is a movement of the tail upward far enough to get it out of the region affected by the slipstreams. However,

results of surveys (not shown in this report) indicate that a 3-inch vertical movement on the model (30-in. full-scale) would be required for any appreciable improvement. This would put the tail well up on the vertical fin. A second solution would be a change in the incidence of the nacelle so as to minimize the intense downwash behind it at high angles of attack. Model construction did not permit tests of such a modification. This change would be accompanied by two other favorable effects. The inclination of the thrust axis would cause the thrust to give a diving moment and would also decrease the downwash in the slipstream itself (both effects would increase stability).

The shift in the regions of downwash noted above is caused by the "shearing" of the upper and lower halves of the slipstream after it has passed over the wing (noted by other observers; see references 3 and 4). An attempt to compute the amount of this shift has been made, after the manner of reference 4. It is assumed that the vertical components of the rotational velocity are completely damped out as they pass over the wing, leaving the lateral components only, which cause the translation of the upper half of the slipstream in one direction and the lower half in the other. The circular-velocity contours are distorted into oval shapes.

Actual computation of this shift of necessity involves a number of assumptions and the neglect of secondary variables. The computation was made as follows: The trapezoidal-torque and thrust-grading curves of figure 15 were assumed. These would give velocity contours immediately behind the propeller (and before passing over the wing) as shown by the dotted lines in figure 16(a) for a T_c of 0.131. Downwash contours due to the pitch angle of the propeller axis also would be circular. Figure 16(b) shows these contours computed by the method of reference 5, with the additional refinement of assuming a trapezoidal distribution of downwash across the diameter of the slipstream and taking into account the average upwash in front of the wing (which adds to the effective pitch angle of the propeller axis). Note that these contours do not include the downwash component of the rotational velocities in the slipstream. The solid lines of figures 16(a) and (b) show the distorted contours in the region of the tail, based on the assumption outlined above that the vertical components of the rotational velocity (computed from the assumed torque grading) are completely damped out by the wing.

These downwash angles (ϵ_p) due to the slipstream were superimposed on the downwash angles (ϵ_w) due to the wing (computed from reference 6). The location of the tail in the slipstream was then computed in the manner shown diagrammatically in figure 17, where ϵ_p was taken as the average slipstream downwash.

The downwash distribution across the tail span computed by the above method is shown for a range of angles of attack and T_c in figure 18(a) for both propellers rotating down toward the fuselage and in figure 18(b) for both propellers rotating up toward the fuselage. Inspection of these curves indicates that a fair approximation of the shift of the slipstream due to the shearing effect is obtained. The fact that the experimental results exceed the computed results, despite the extreme assumptions made in the computations, indicates that secondary effects, possibly the effect of the nacelles and fuselage and the increase in thrust and torque on the downcoming blade of the pitched propeller are important.

Downwash computations made in the manner outlined above and integrated across the tail span were used to determine the variation of ϵ_{av} versus α, shown on figure 19. The difference between the computed and the observed downwash is due almost entirely tc the increased downwash near the fuselage and behind the nacelles. Better agreement is obtained, however, on the slope $\frac{d\epsilon}{d\alpha}$, which is one of the factors on which $\frac{dC_m}{dC_L}$ will depend. Computed values of $\frac{d\epsilon}{d\alpha}$ are approximately the same as test values.

A comparison of the average downwash determined from an integration of the point-by-point surveys with that determined from the angle of zero lift of the tail is of interest. Figures 12 and 13 show that the point-by-point method measures both higher absolute values of ϵ and higher slopes ($d\epsilon/d\alpha$). The tail would be expected to "weight" its average of ϵ on the basis of $(q/q_o)_{local}$ and c_{local}. Both of these effects, however, would work in the opposite direction to the one observed, since high ϵ occurs in the region of high q/q_o and large chord, and the average ϵ determined by the tail should be higher than that determined from the point-by-point aver-

age. Apparently the "jet" effect of the slipstream and the extreme variation in downwash combine to make the tail minimize the imposed changes in angle. The qualitative conclusion may be reached that the changes in stability which would be predicted from local flow conditions over a tail in the slipstream will be conservative, that is, they will exaggerate the effect.

The tendency of the tail to minimize the effect of local flow changes is also shown by the variations in tail-effectiveness factor shown on figure 11(e). The change in $\frac{dC_{m_t}}{dC_L}$ associated with this factor may be deduced from the following relations.

$$C_{m_{tail}} = \frac{l_t}{Sc} \frac{dC_{L_t}}{d\alpha_t} \left[\sum_{-\frac{b_t}{2}}^{\frac{b_t}{2}} \alpha_t \; q/q_o \; c_l \right] \tag{1}$$

$$\frac{dC_{m_t}}{dC_L} = - \frac{l_t b_t}{Sc} \frac{dC_{L_t}}{d\alpha_t} \frac{d\left[\frac{\Sigma \alpha_t \; q/q_o \; c_l}{b_t}\right]}{d\alpha} \frac{d\alpha}{dC_L} \tag{2}$$

$$\frac{dC_m}{dC_L} = -1.0 \frac{dC_{L_t}}{d\alpha_t} \frac{d\alpha}{dC_L} \frac{d[\text{average T.E.F.}]}{d\alpha} \tag{3}$$

Table I compares the $\frac{dC_{m_t}}{dC_L}$ computed by equation (3) with that actually measured in the force tests.

TABLE I

Computed					Force test			
Direction of propeller rotation	$\frac{dTEF}{d\alpha}$	$\frac{dC_{L_t}}{d\alpha_t}$	$\frac{d\alpha}{dC_L}$	$\frac{dC_{m_t}}{dC_L}$		$\frac{dC_{m_t}}{d\alpha}$	$\frac{d\alpha}{dC_L}$	$\frac{dC_{m_t}}{dC_L}$
(1)	0.214	0.066	10.65	-0.151	↷ ↷	-0.0179	10.25	-0.184
(2)	.441	↓	↓	-.310	↗ ↖	-.0211	10.00	-.211
(3)	.189	↓	↓	-.133	↷ ↶	-.0107	11.32	-.121
Propeller off	.353	↓	13.50	-.315	Propeller off	-.0209	12.10	-.253

The same trend is observable in both, but the computed values predict a greater effect of power than was actually measured.

CONCLUSIONS

1. The greatest single effect of power on the longitudinal stability of the XB-28 is due to the shift of the intense regions of downwash behind the nacelles. This shift is most favorable for both propellers rotating up toward the fuselage, giving approximately the same $\frac{dC_m}{dC_L}$ as power off. With the opposite rotation the airplane becomes slightly unstable at high angles of attack. The customary direction of rotation, both propellers right hand, has an intermediate effect.

2. The theory fails in the computation of the absolute value of downwash because of the neglect of the effects of the nacelle and fuselage. Fair agreement, however, is obtained for $\frac{d\epsilon}{d\alpha}$.

Ames Aeronautical Laboratory,
National Advisory Committee for Aeronautics,
Moffett Field, Calif.

REFERENCES

1. Rogallo, Francis M., and Swanson, Robert S.: Power-On Wind-Tunnel Tests of the Longitudinal Stability and Control Characteristics of the 1/10-Scale Model of the North American XB-28 Airplane in the 7- by 10-Foot Wind Tunnel. NACA C.M.R., June 1941.

2. Silverstein, Abe, Katzoff, S., and Bullivant, W. Kenneth: Downwash and Wake behind Plain and Flapped Airfoils. Rep. No. 651, NACA, 1939.

3. Stiess, W.: Effect of Direction of Propeller Rotation on the Longitudinal Stability of Twin-Engine Airplanes. Jahrb. 1938 der deutschen Luftfahrtforschung, pp. I 206-219. R. Oldenbourg (Munich).

4. Bryant, L. W., and McMillan, G. A.: The Longitudinal Stability of a Twin-Engined Monoplane with Airscrews Running. British A.R.C., Stability and Control Sub-Committee 3603 (S. & C. 971), June 28, 1938.

5. Goett, Harry J., and Pass, H. R.: Effect of Propeller Operation on the Pitching Moments of Single-Engine Monoplanes. NACA A.C.R., May 1941.

6. Silverstein, Abe, and Katzoff, S.: Design Charts for Predicting Downwash Angles and Wake Characteristics behind Plain and Flapped Wings. Rep. No. 648, NACA, 1939.

NACA

Fig. 1

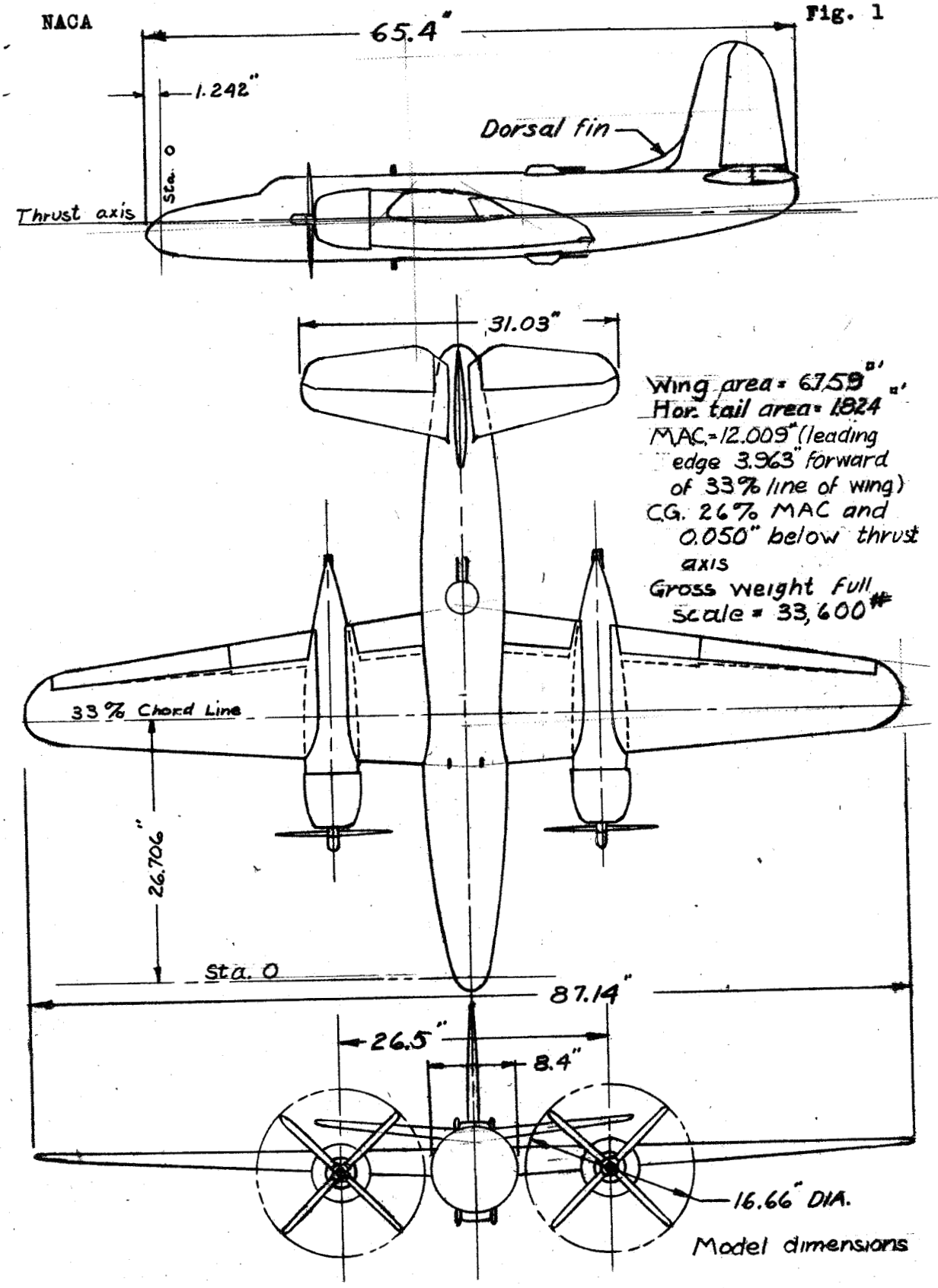

Fig 1. Three view drawing of the 1/8 scale model of the North American airplane XB-28

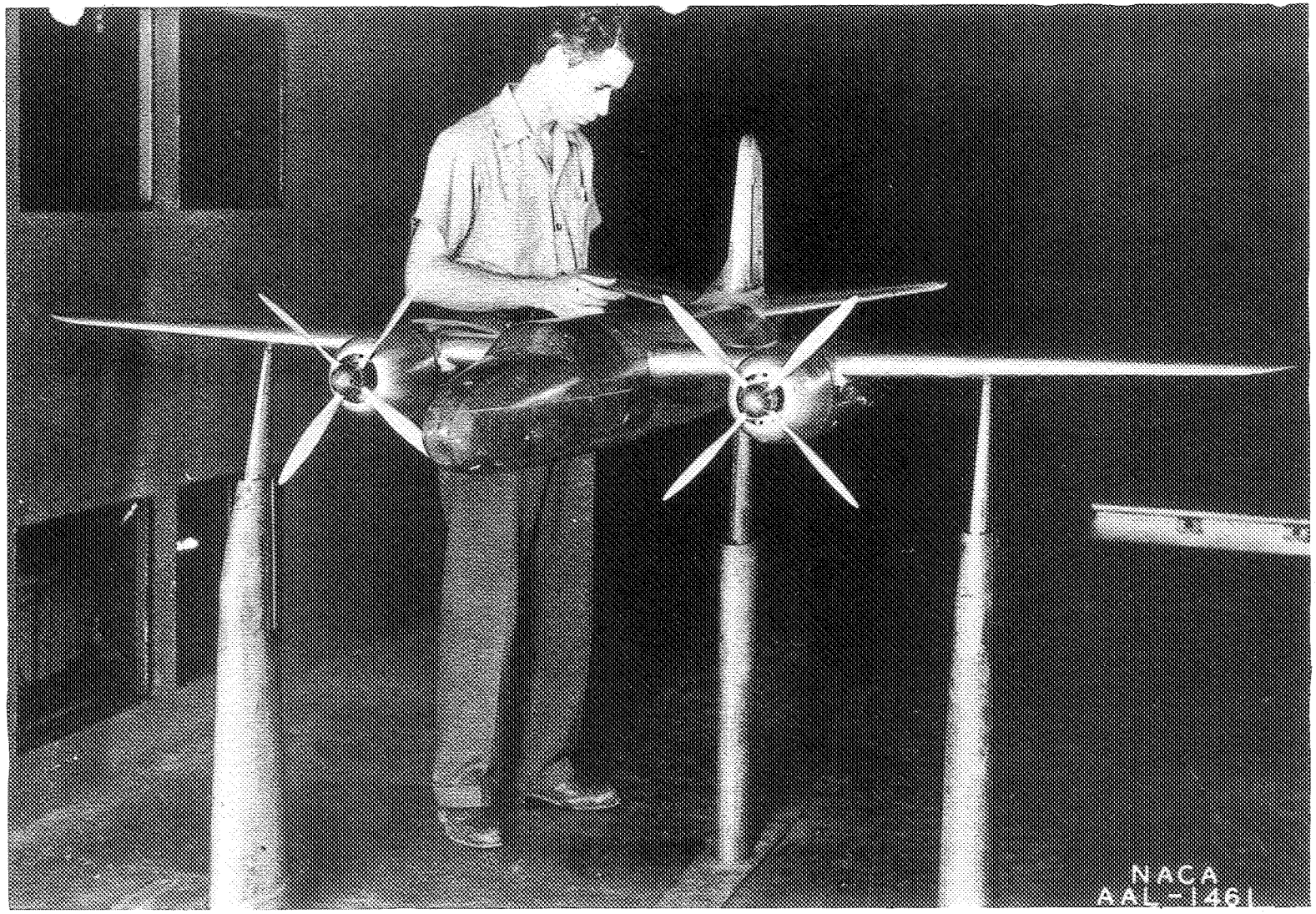

Figure 2.- Force test set-up for 1/10 scale model of North American XB-28 airplane.

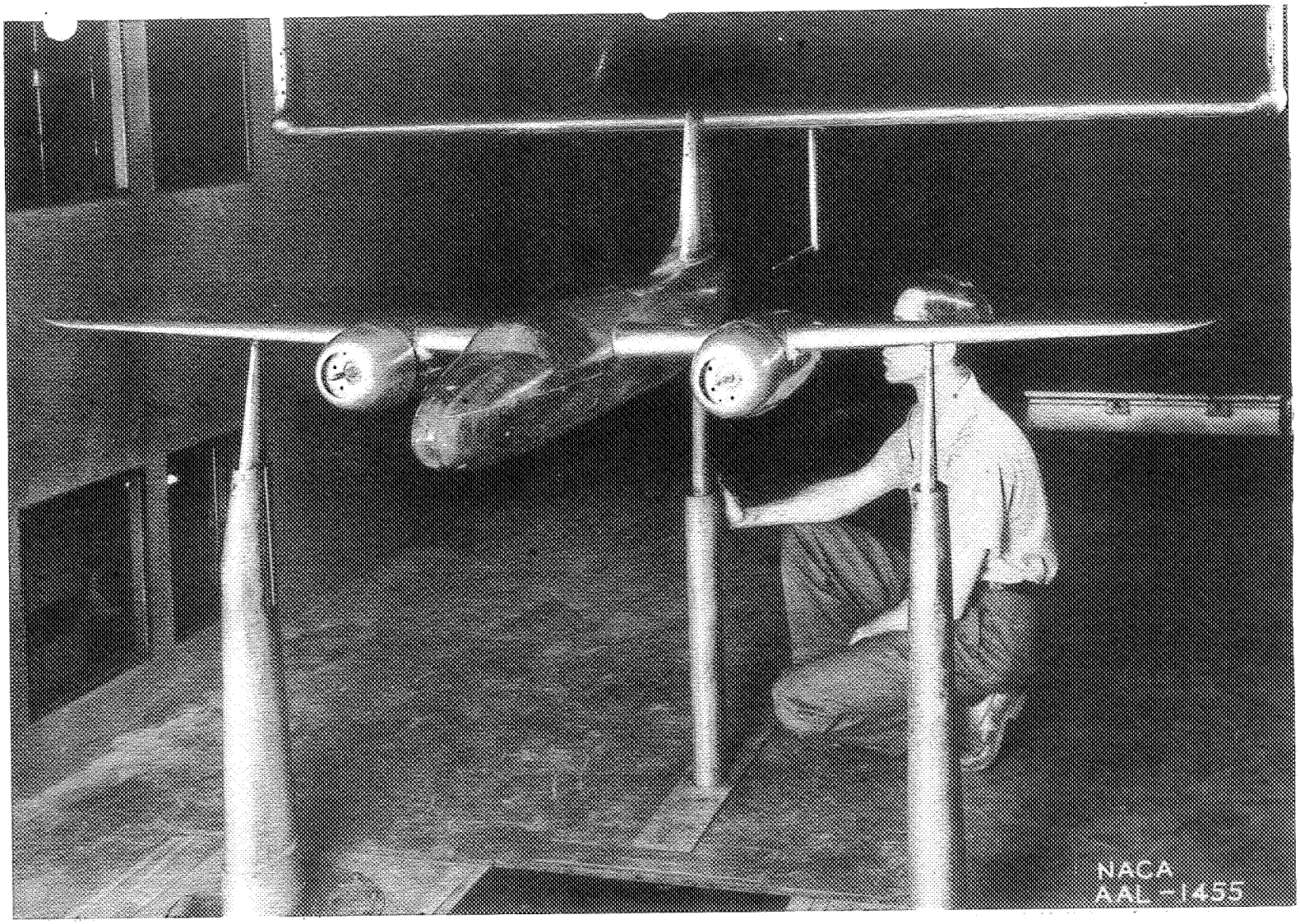

Figure 3.- Point by point survey set up for 1/10 scale model of North American XB-28 airplane.

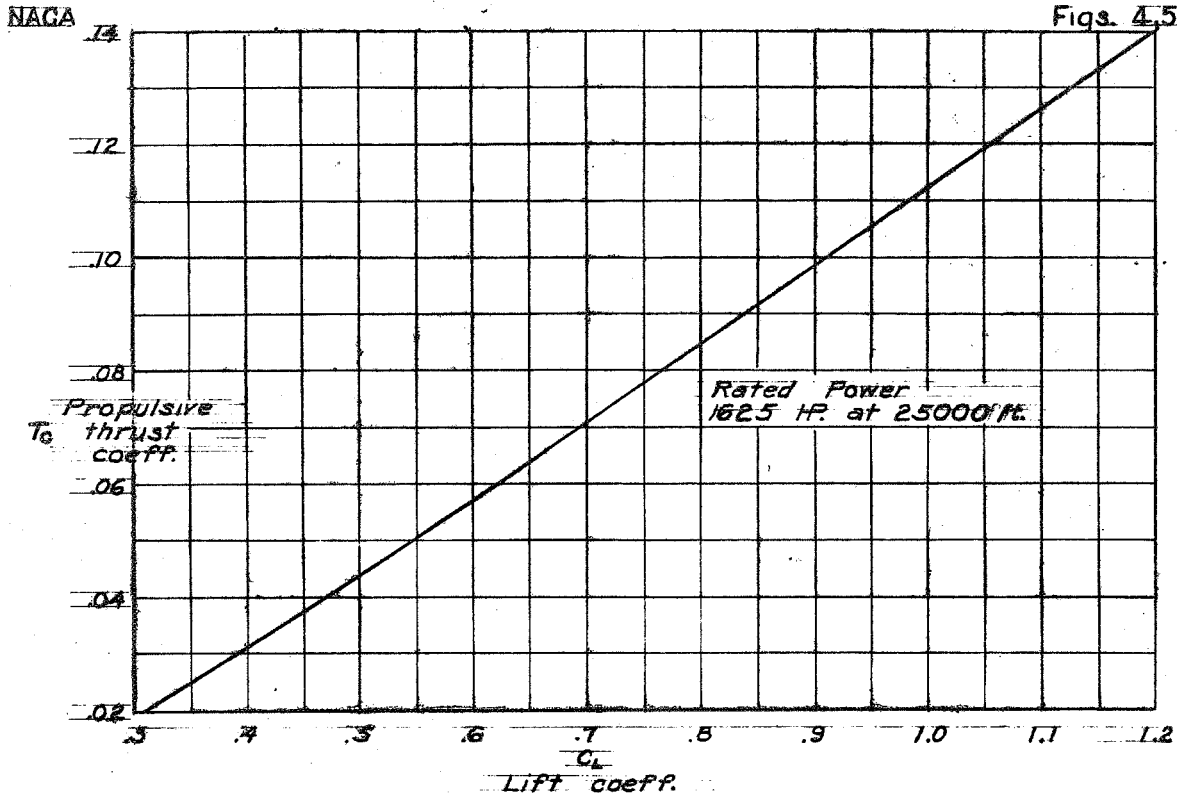

Fig. 4. - Calculated thrust coefficient vs. C_L used in test of the 1/8 scale model XB-28

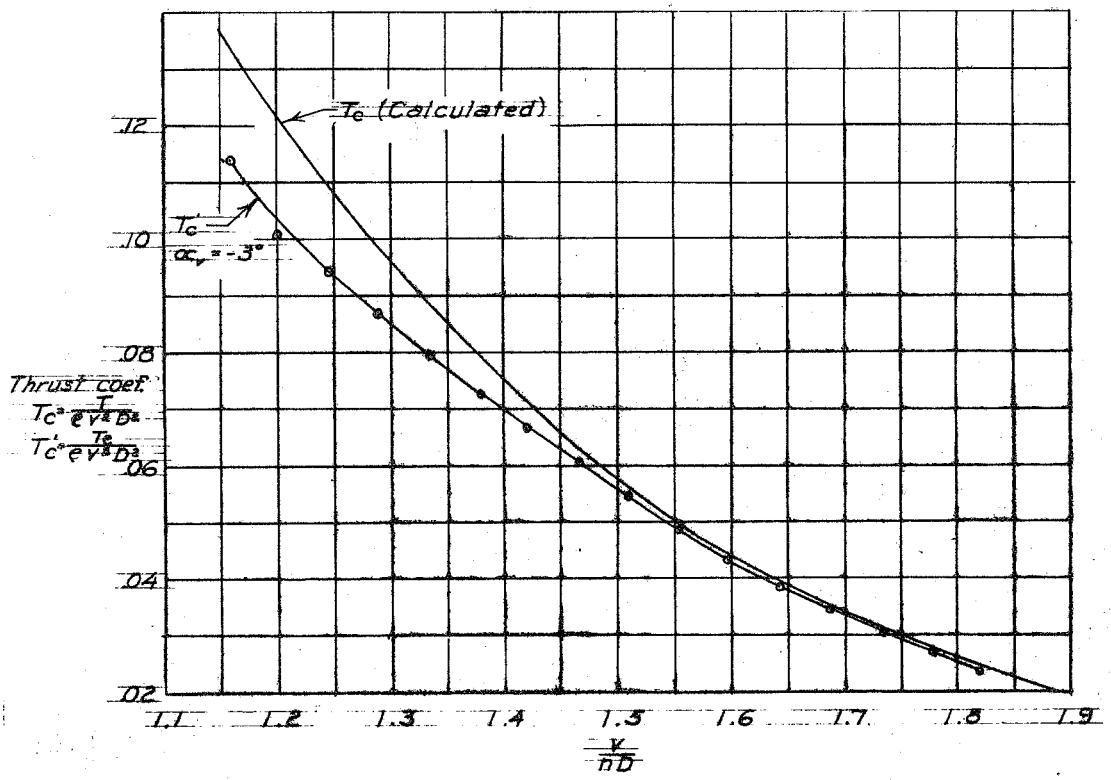

Fig. 5 - β=40.5°. Thrust Coef. v.s. $\frac{V}{nD}$ characteristics of model propeller.

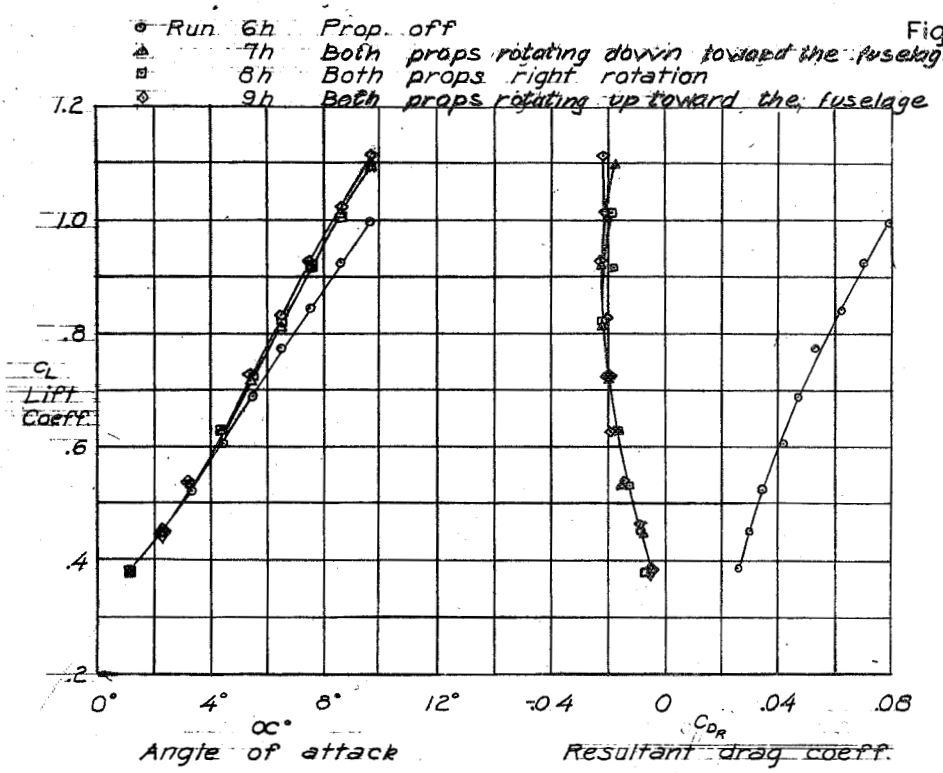

Fig. 6.- Effect of propeller rotation on lift and drag characteristics. Horizontal tail surface removed. Rated power = 1625 horsepower at 25,000 feet, β = 40.5°.

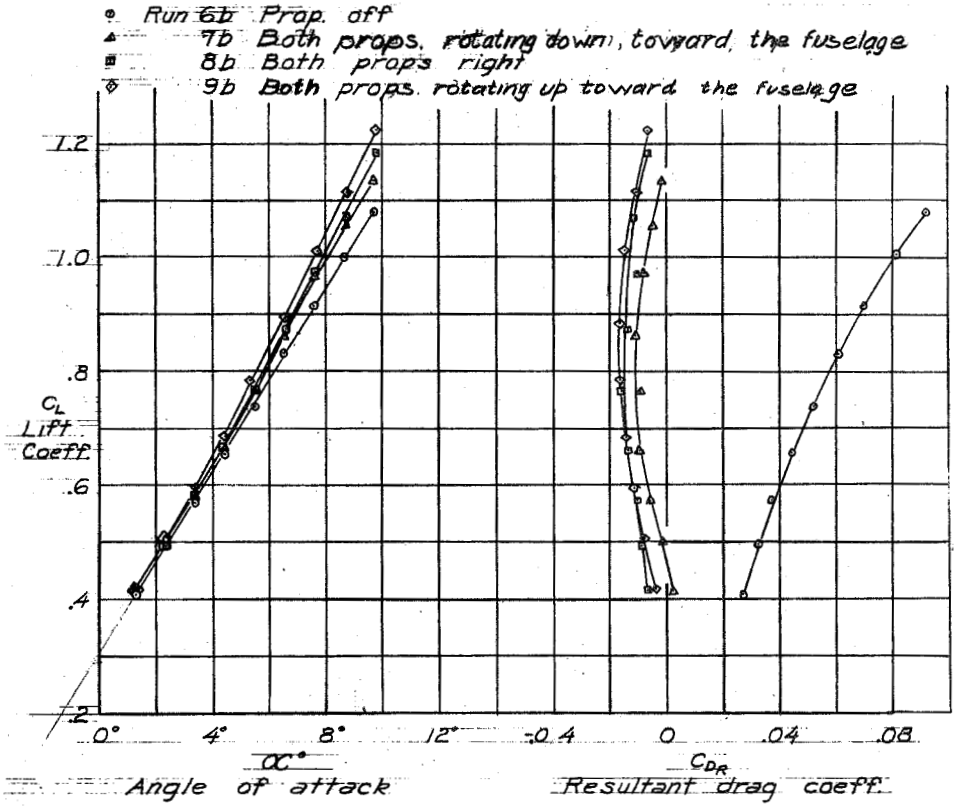

Fig. 7 - Effect of propeller rotation on lift and drag characteristics. Horizontal tail surface on i_t = 1.5°. Rated power = 1625 at 25,000 feet, β = 40.5°.

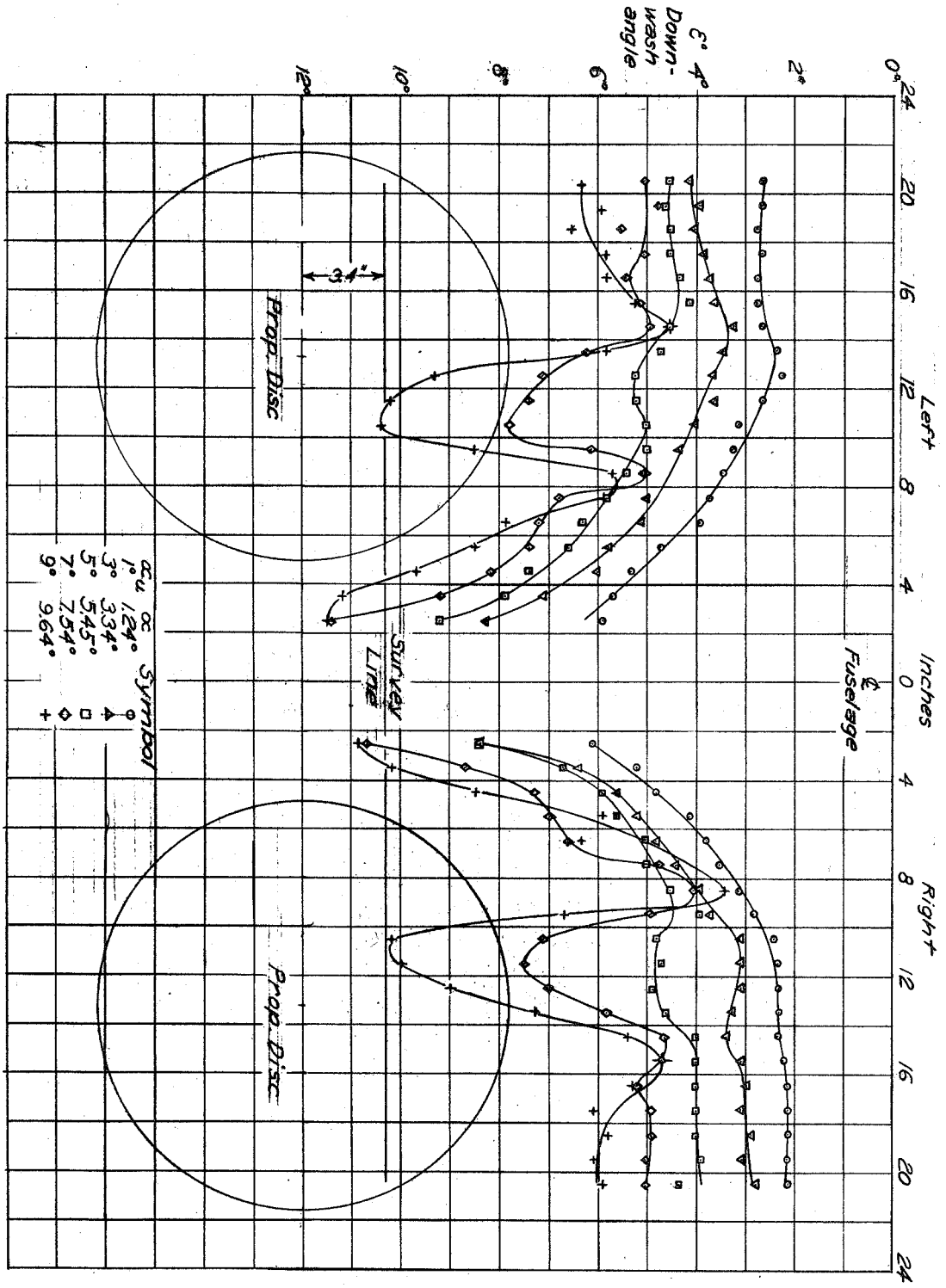

Fig. 8(a) Downwash survey at approximately 25 percent chord line of horizontal tail, power off.

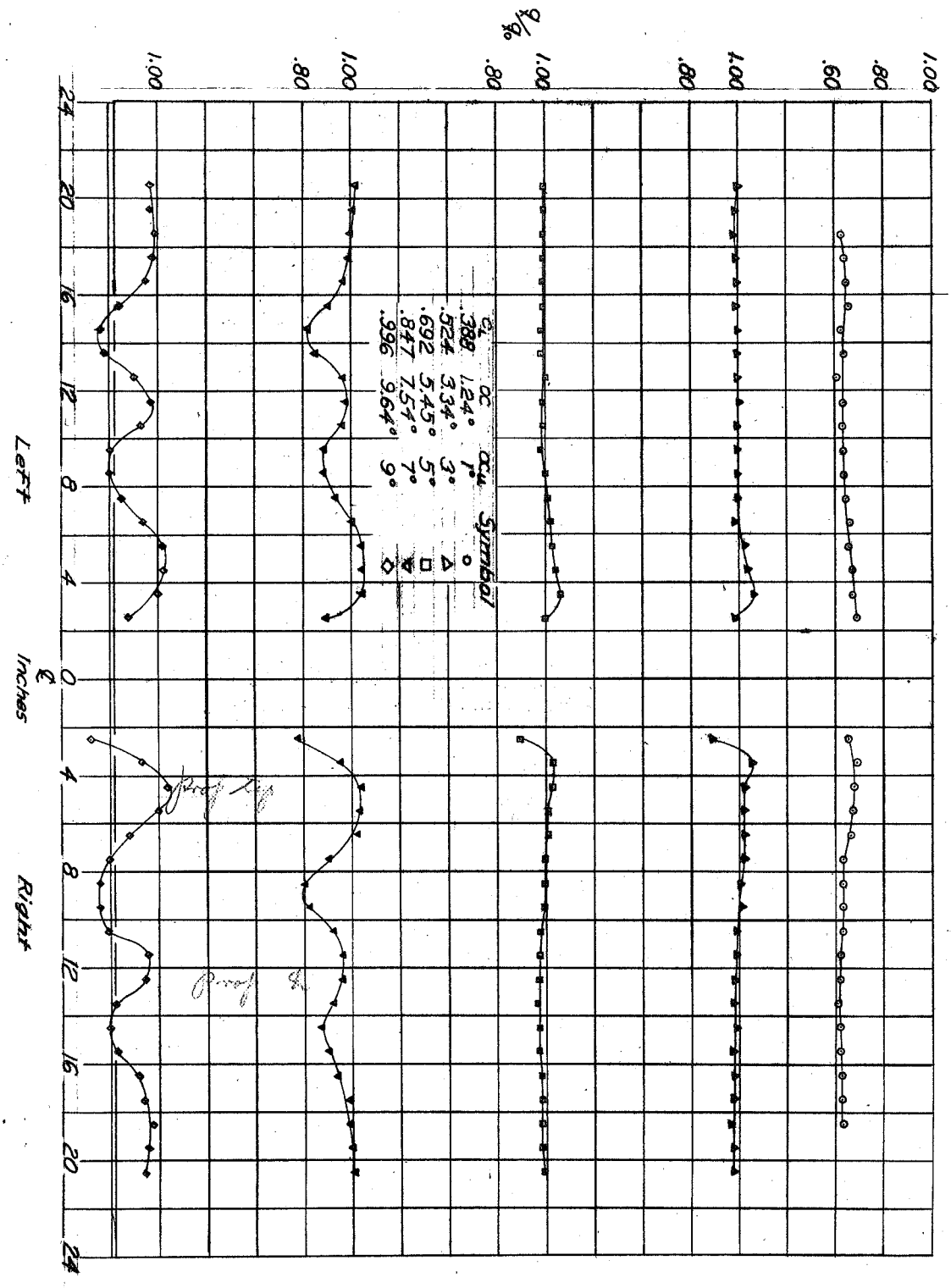

Fig. 8 (b) q/q_0 survey at approximately 25 percent chord line of horizontal tail, power off.

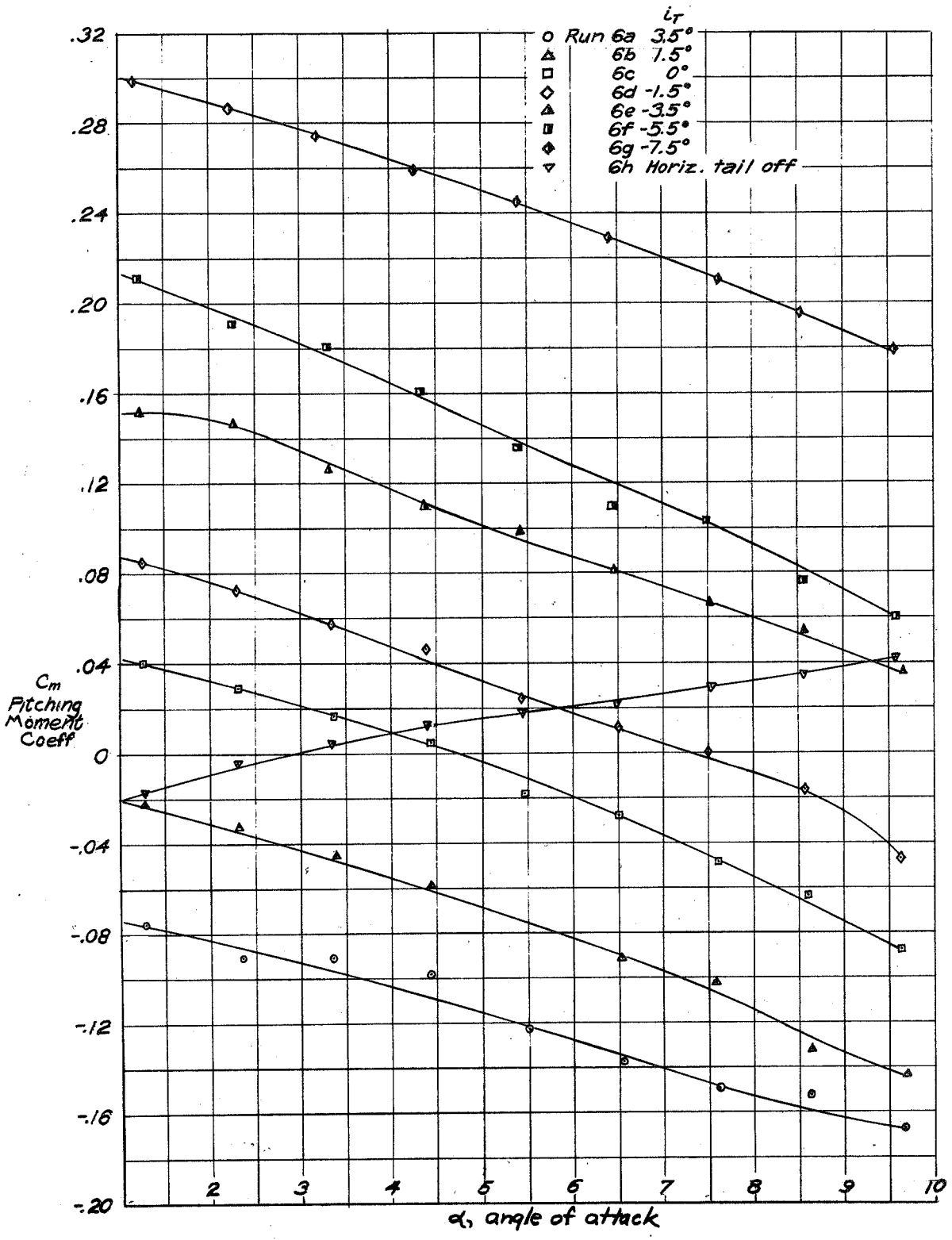

Fig. 8 (c) Effect of stabilizer setting on pitching moment power off.

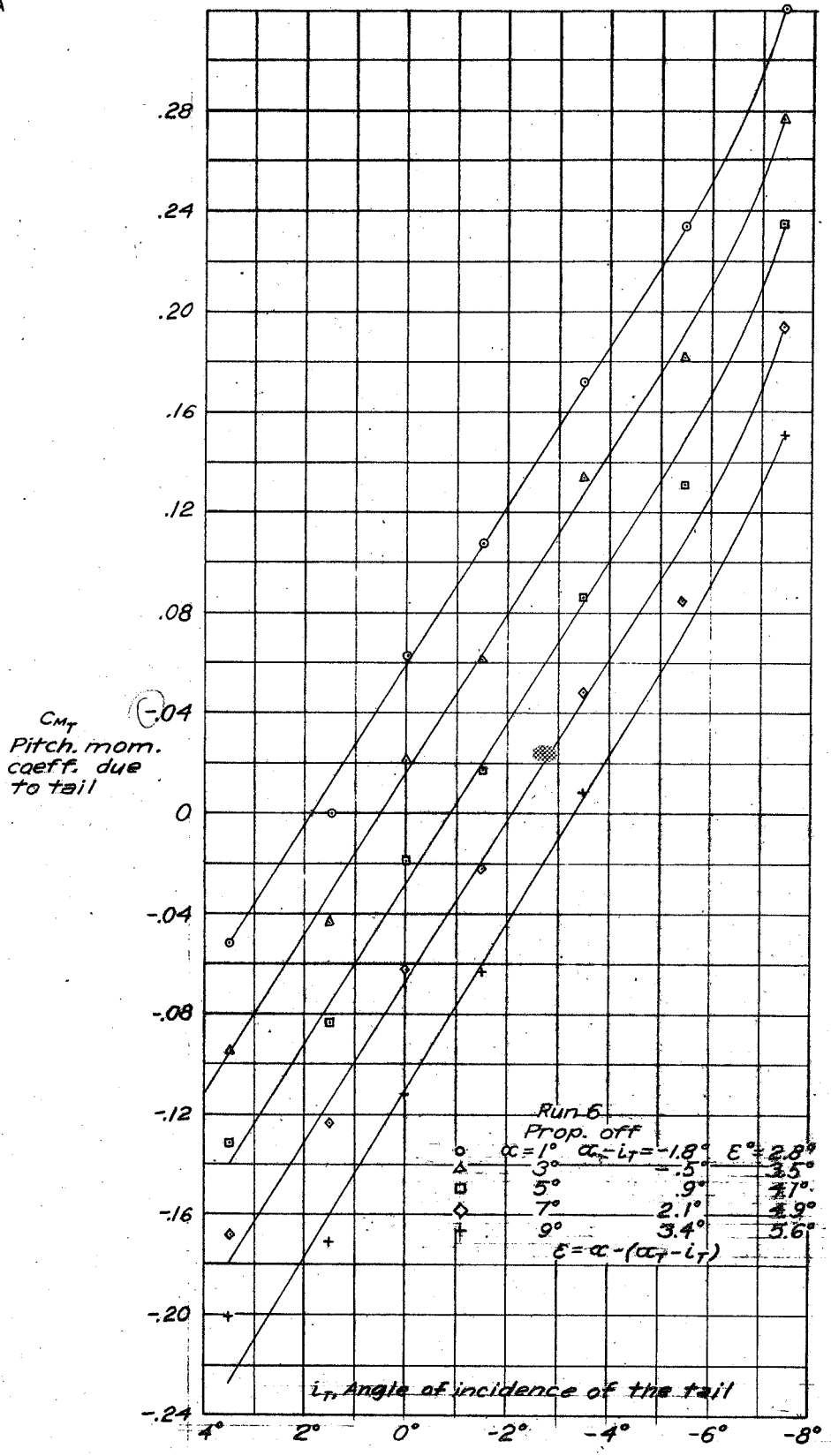

Fig. 8(d) Pitching moment of the horizontal tail surface vs. angle of incidence of the stabilizer-power off.

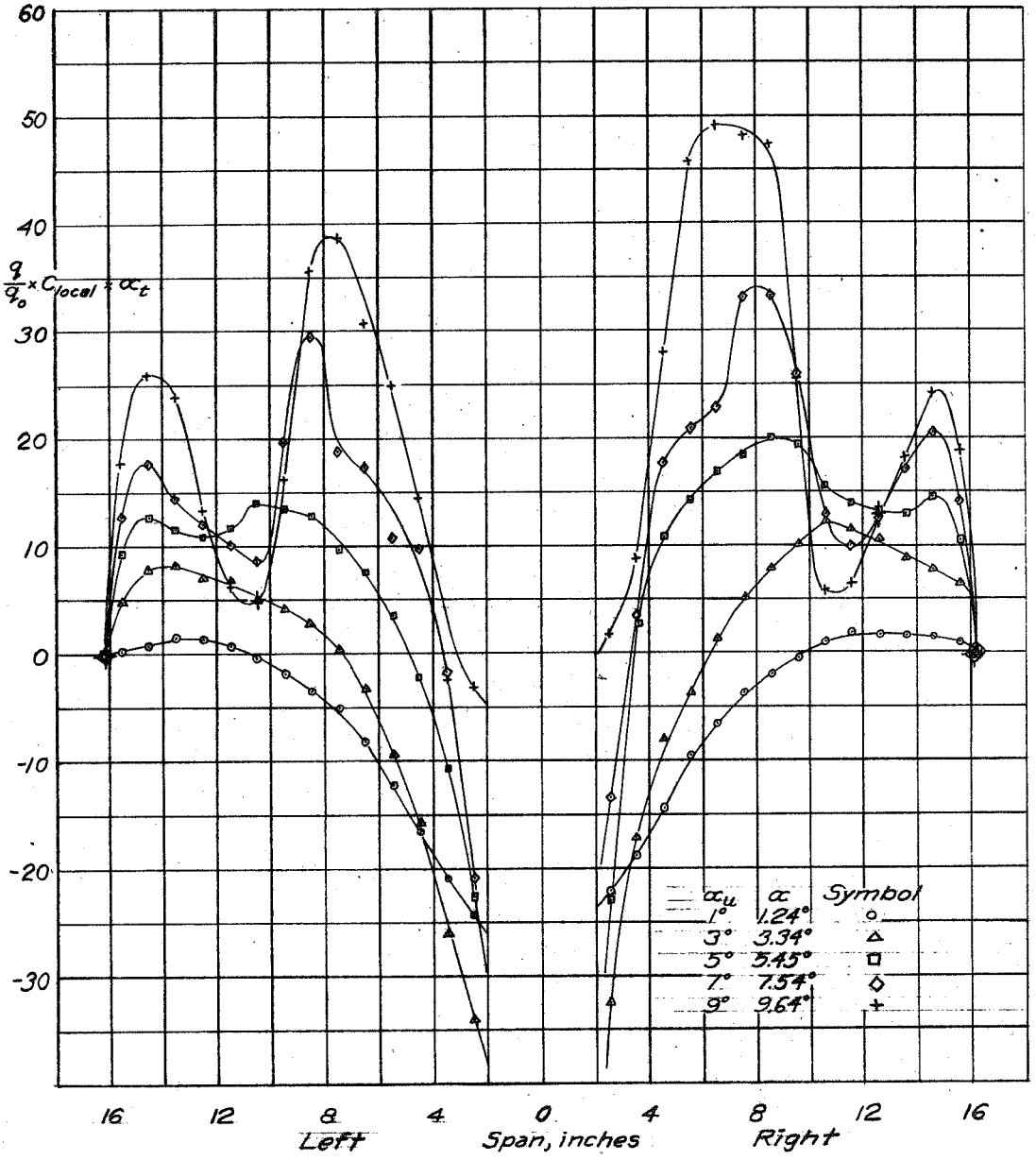

Fig. 8(e) Tail effectiveness factor. Variation of $q/q_o \times C_{local} \times \alpha_t$ across horizontal tail span for $i_t = 1.5°$ -- power off.

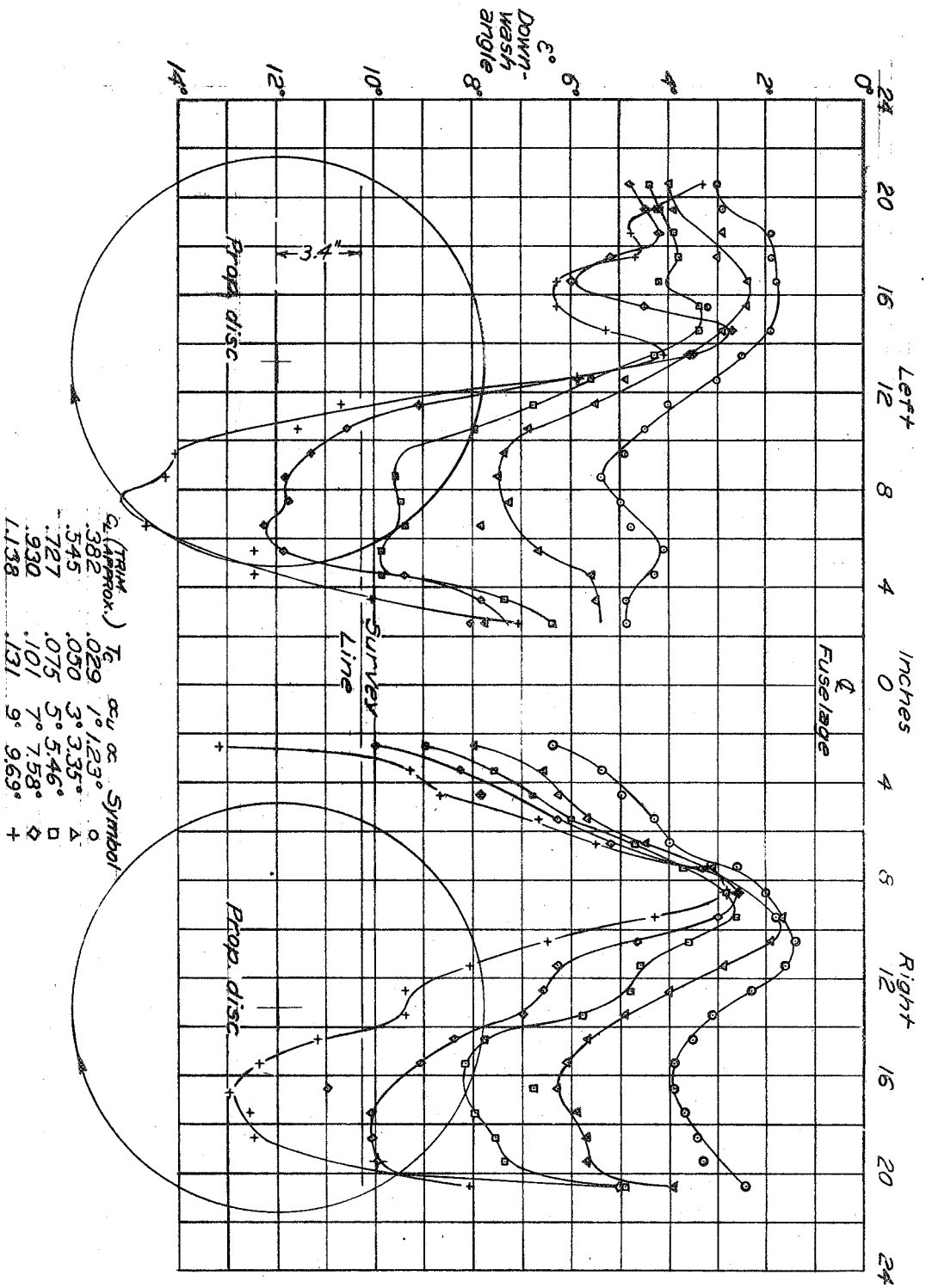

Fig. 9 (a) Downwash survey at approximately 25 percent chord line of horizontal tail. Both propellers right hand rotation. $\beta = 40.5°$. Rated power = 1625 horsepower at 25,000 feet.

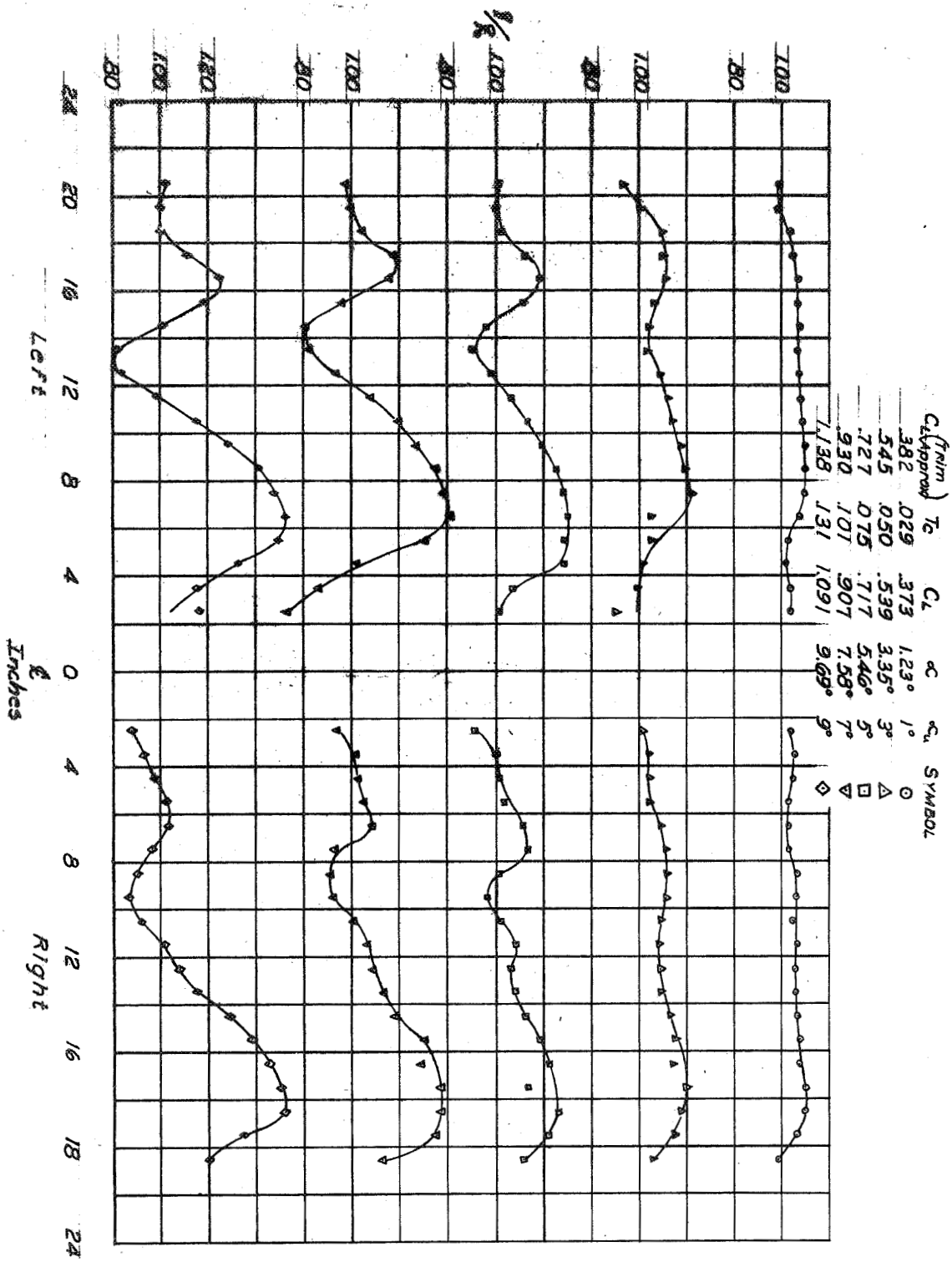

Fig. 9(b) q/q_∞ Survey at approximately 25 percent chord line of horizontal tail. Both propellers right hand rotation, $\beta = 40.5°$

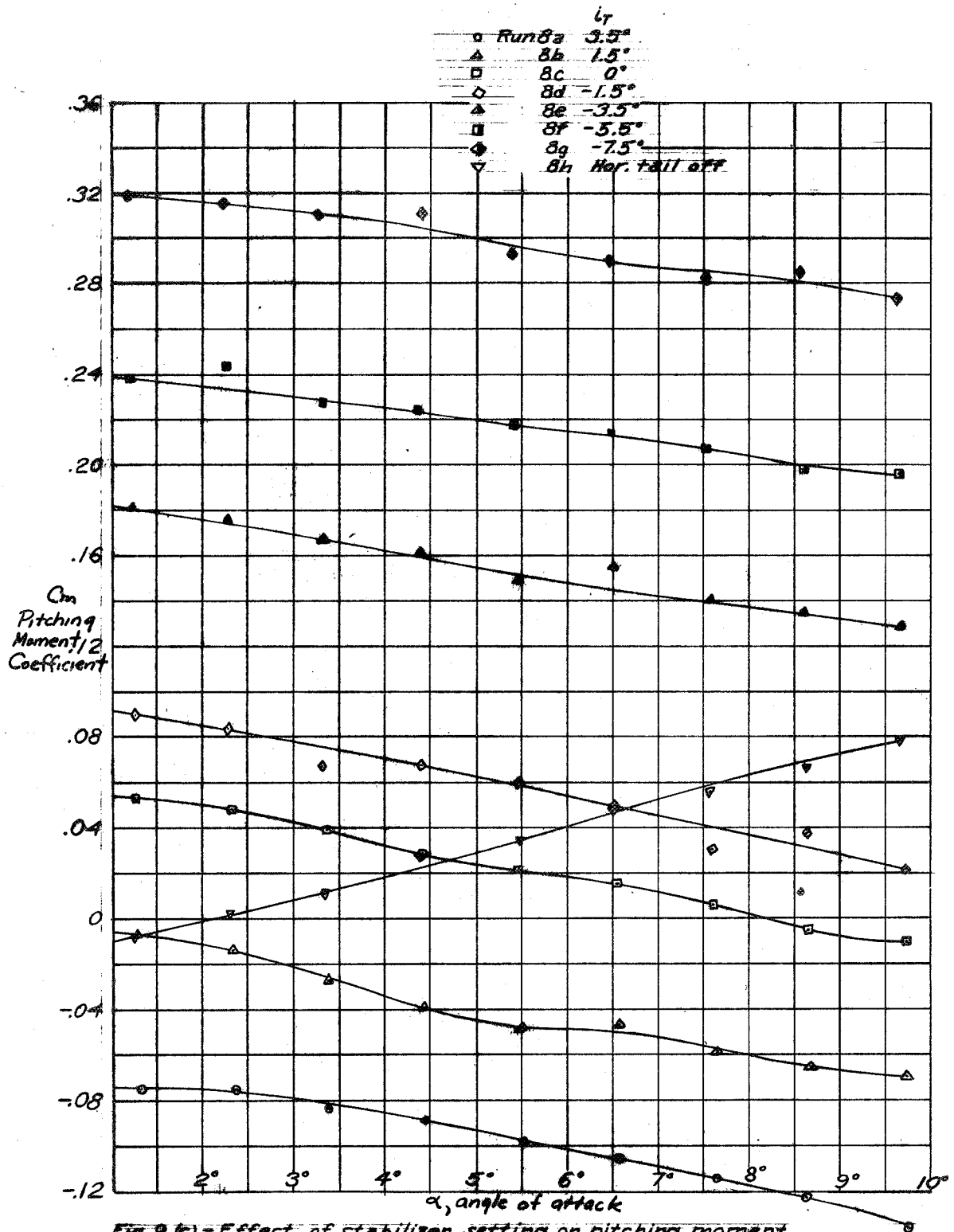

Fig. 9 (c) - Effect of stabilizer setting on pitching moment.
Both propellers right hand rotation. β = 40.5°.
Rated power = 1625 horsepower at 25,000 feet.

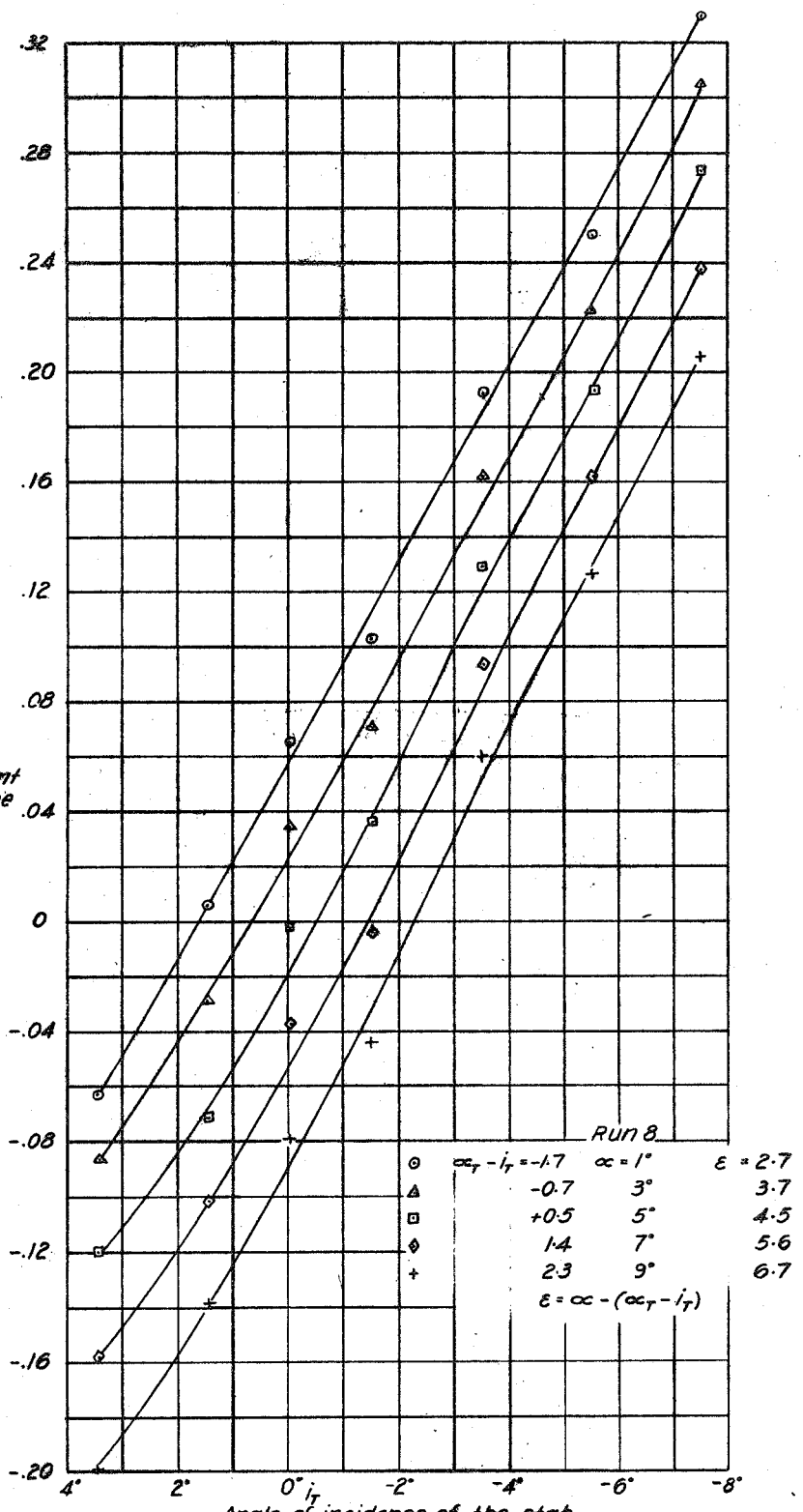

Fig. 9d Pitching moment of the horizontal tail surface vs. angle of incidence of the stabilizer. Both propellers right hand rotation. β = 40.5°. Rated power - 1625 horse power at 25,000 feet.

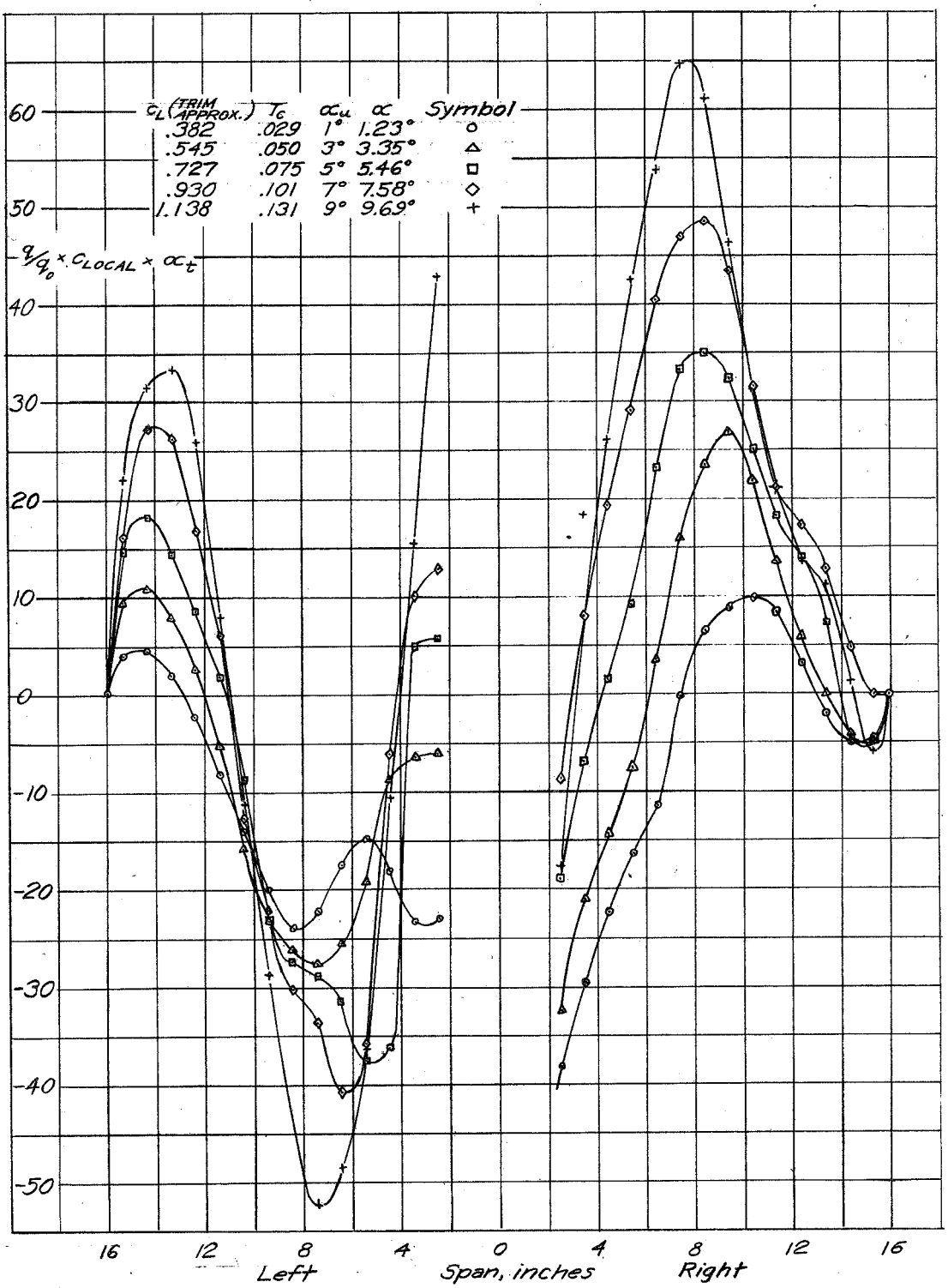

Fig. 9(e)- Tail effectiveness factor. Variation of $q/q_0 \times C_{LOCAL} \times \alpha$ across horizontal tail span for $i_t = 1.5°$. Both propellers right hand, $\beta = 40.5°$

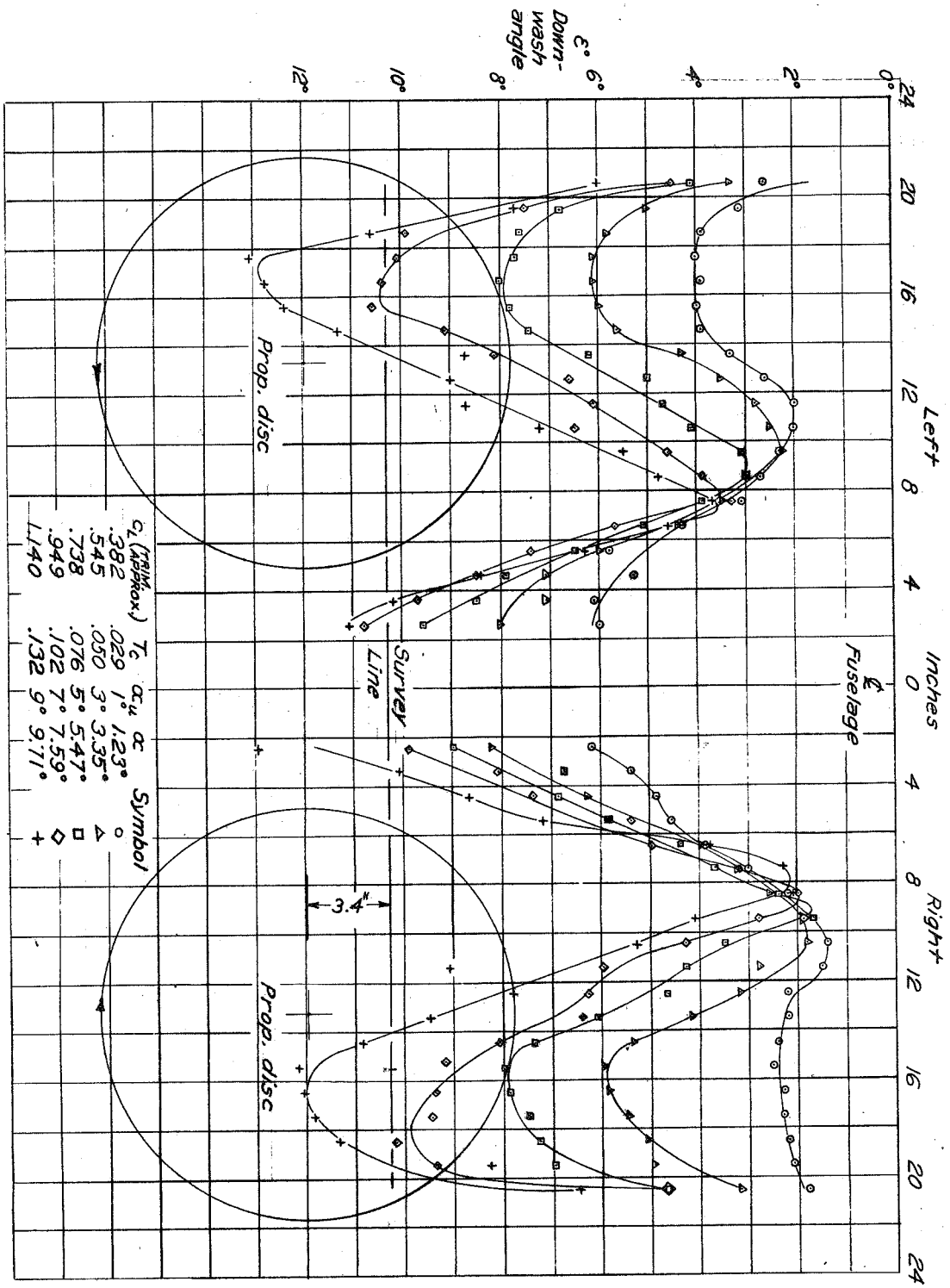

Fig. 10 (a) Downwash survey at approximately 25 percent chord line of horizontal tail. Both propellers rotating up toward the fuselage. β = 40.5° Rated power = 1625 horsepower at 25,000 feet.

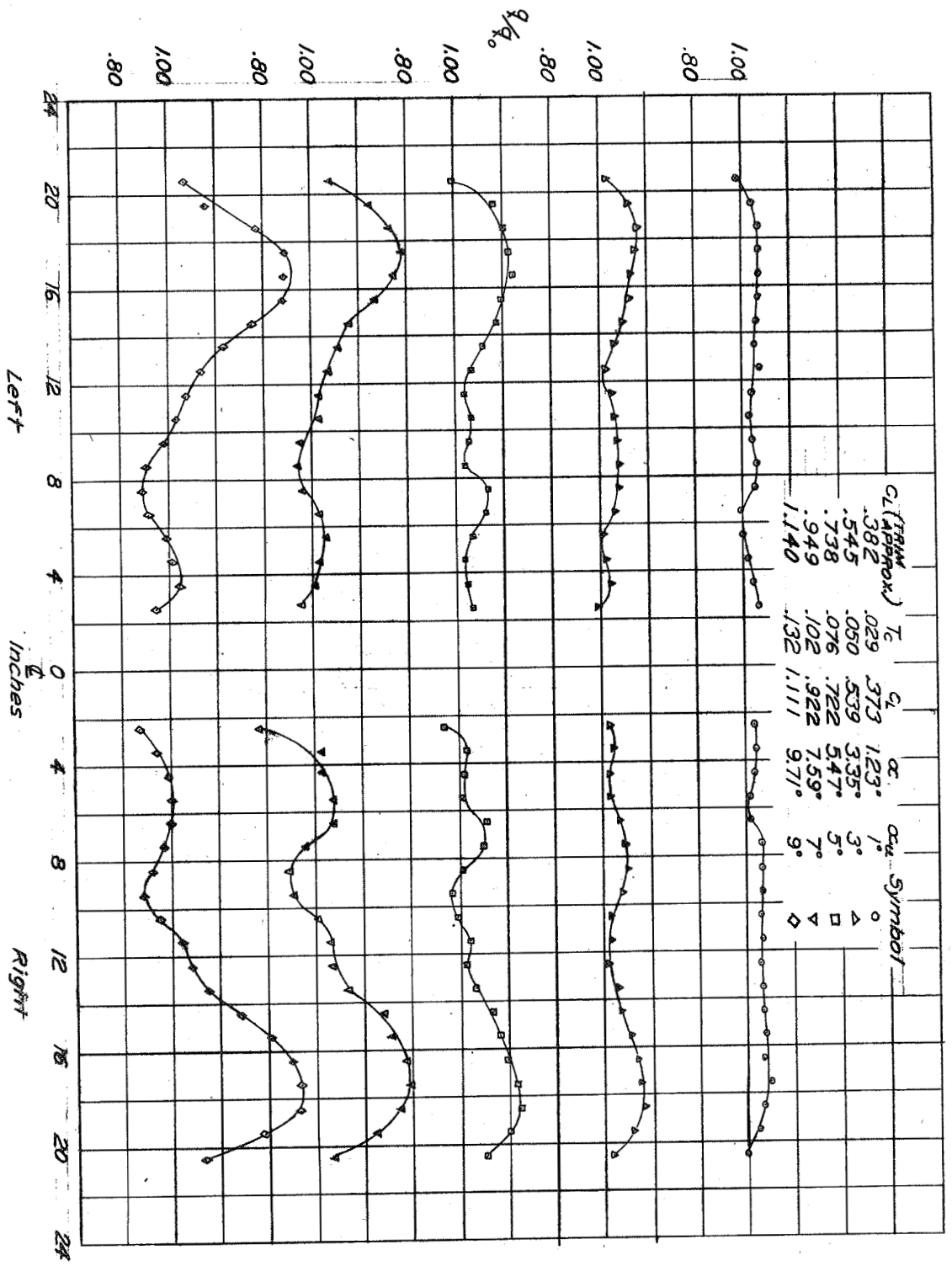

Fig. 10(b) q/q∞ survey at approximately 25 percent chord line of horizontal tail. Both propellers rotating up toward the fuselage. β = 40.5°

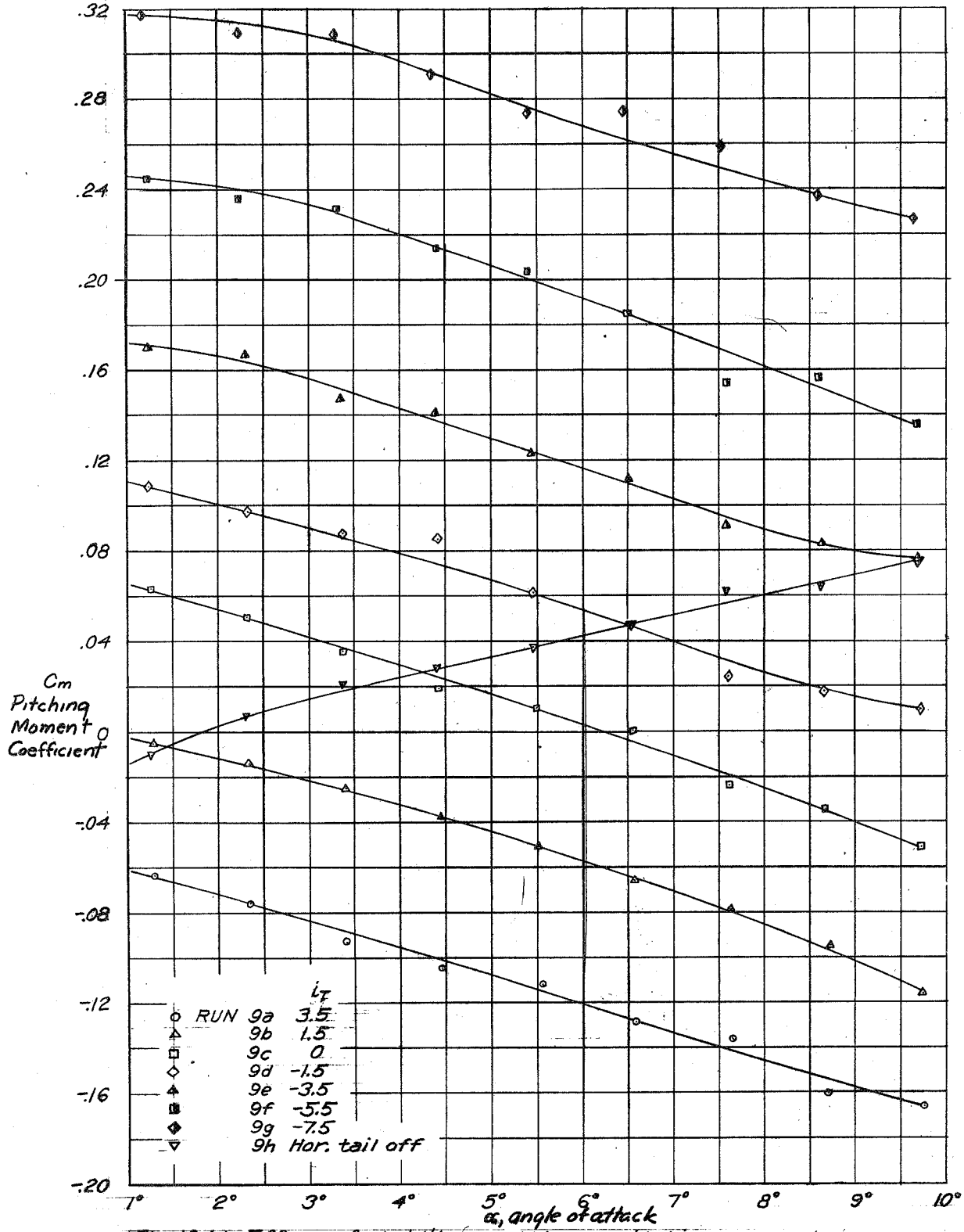

Fig. 10 (c) Effect of stabilizer setting on pitching moment. ~~Both propellers rotating up toward the fuselage.~~ $\beta = 40.5°$. Rated power = 1625 horsepower at 25,000 feet.

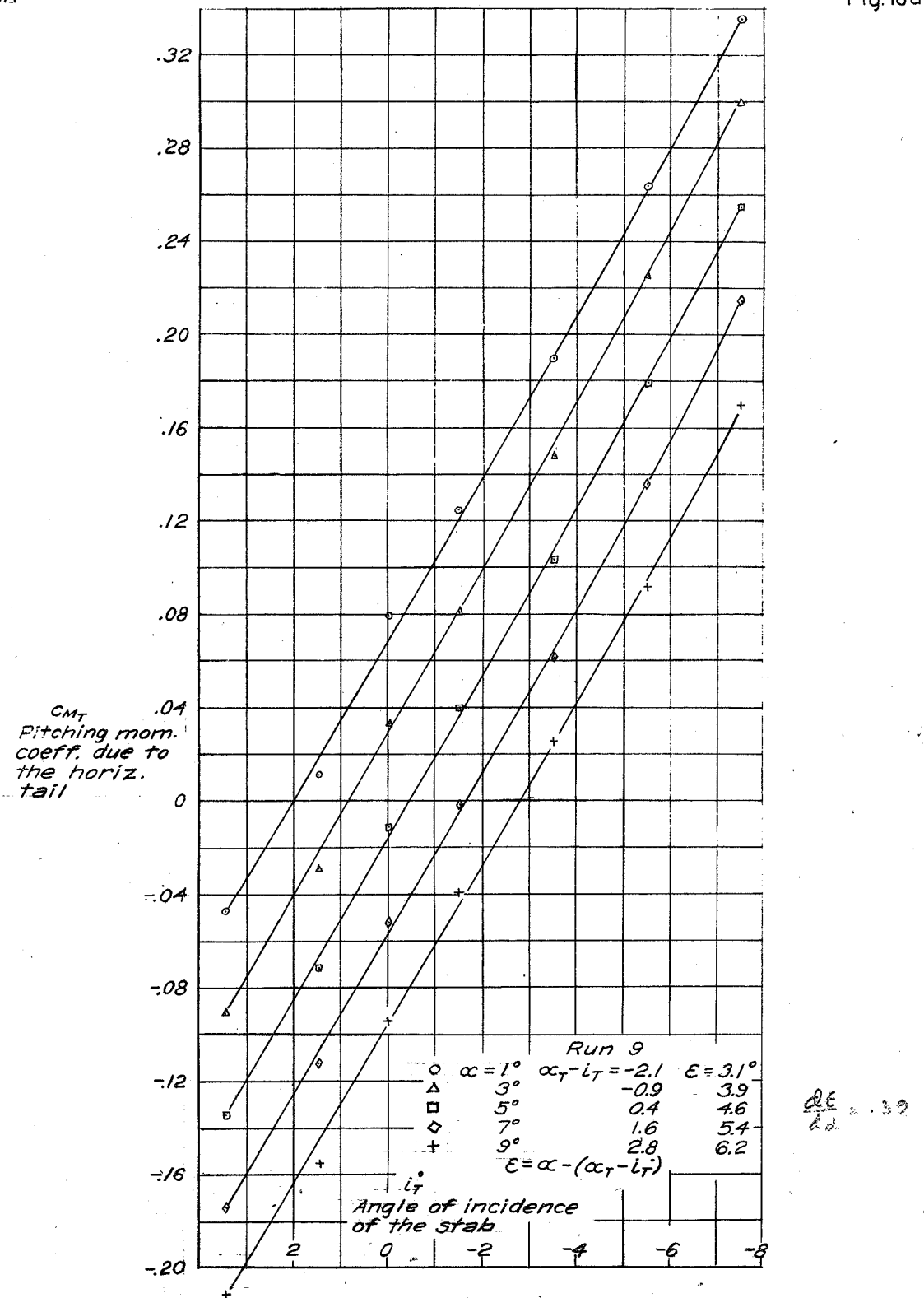

Fig. 10(d) Pitching moment of the horizontal tail surface vs. angle of incidence of the stabilizer. Both propellers rotating up toward the fuselage. β = 40.5°. Rated power = 1625 horsepower at 25,000 feet.

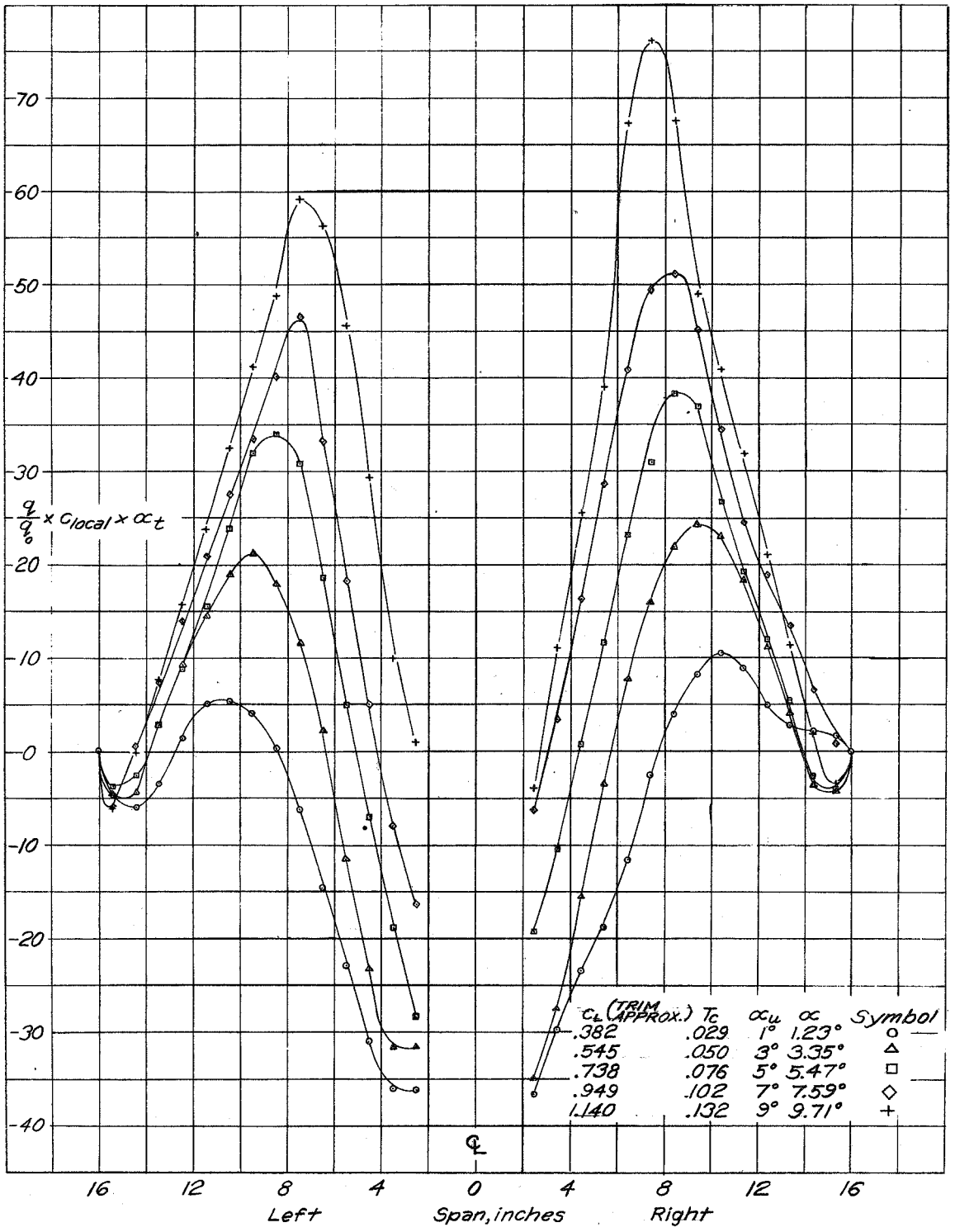

Fig. 10 (e) Tail effectiveness factor. Variation of $q/q_o \times c_{local} \times \alpha_t$ across horizontal tail span for $i_t = 1.5°$. Both propellers rotating up toward the fuselage. $\beta = 40.5°$
Rated power = 1625 horse power at 25,000 feet.

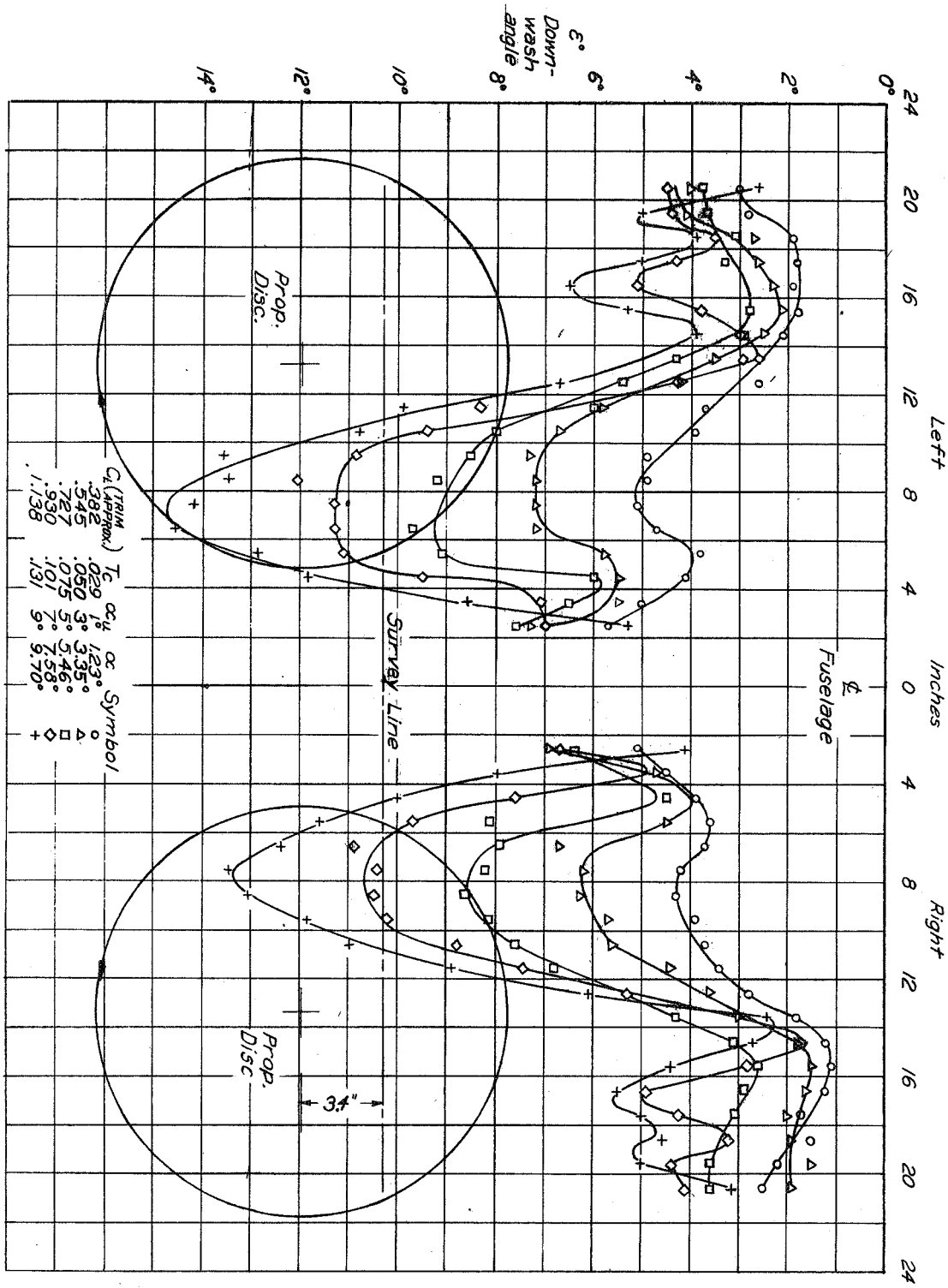

Fig. 11(a) Downwash survey at approximately 25 percent chord line of horizontal tail. Both propellers rotating down toward the fuselage. β = 40.5°. Rated power = 1625 horsepower at 25,000 feet.

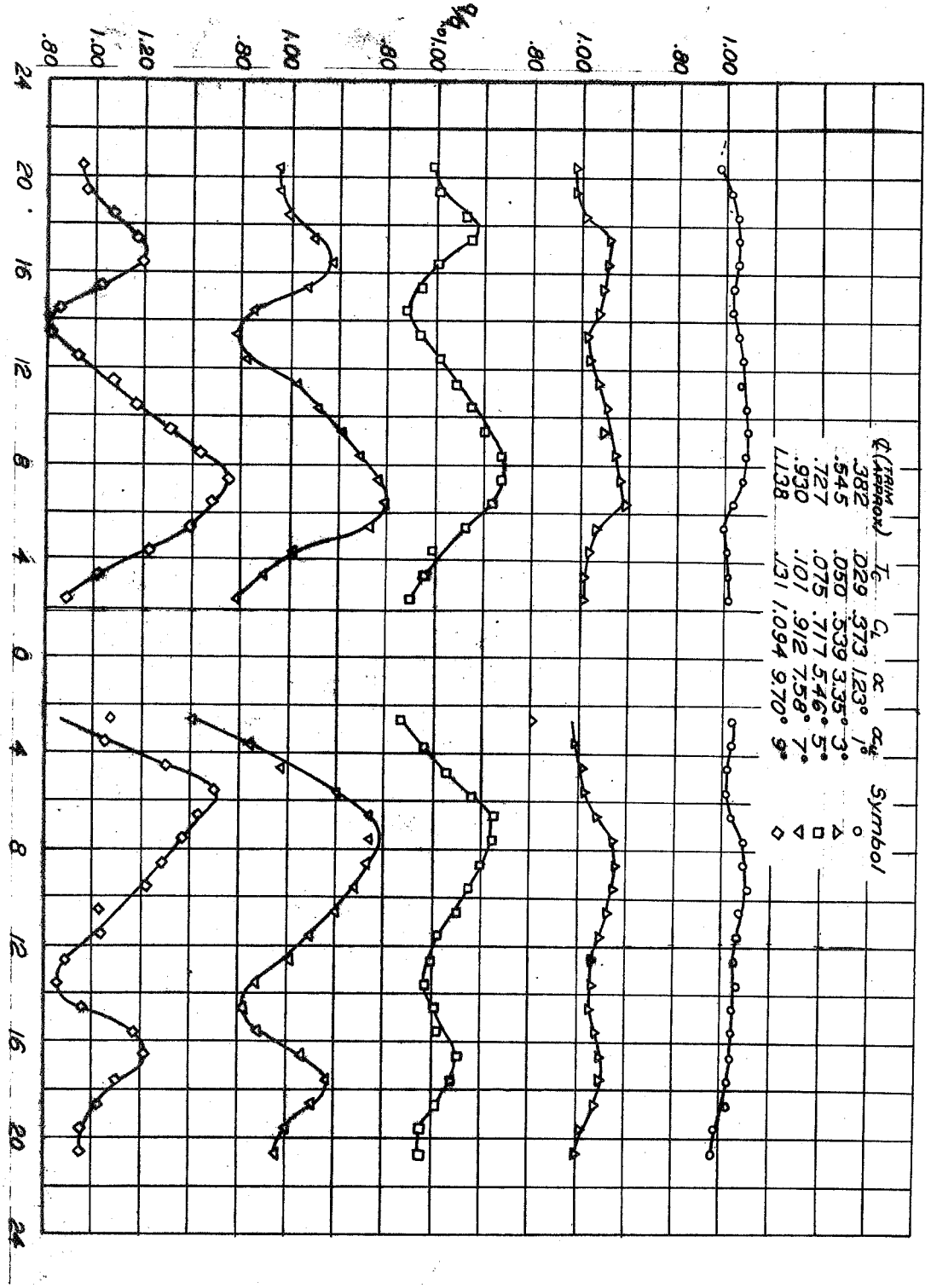

Fig. 11(b) q/q_∞ survey at approximately 25 percent chord line of horizontal tail. Both propellers rotating down toward the fuselage $\beta = 40.5°$

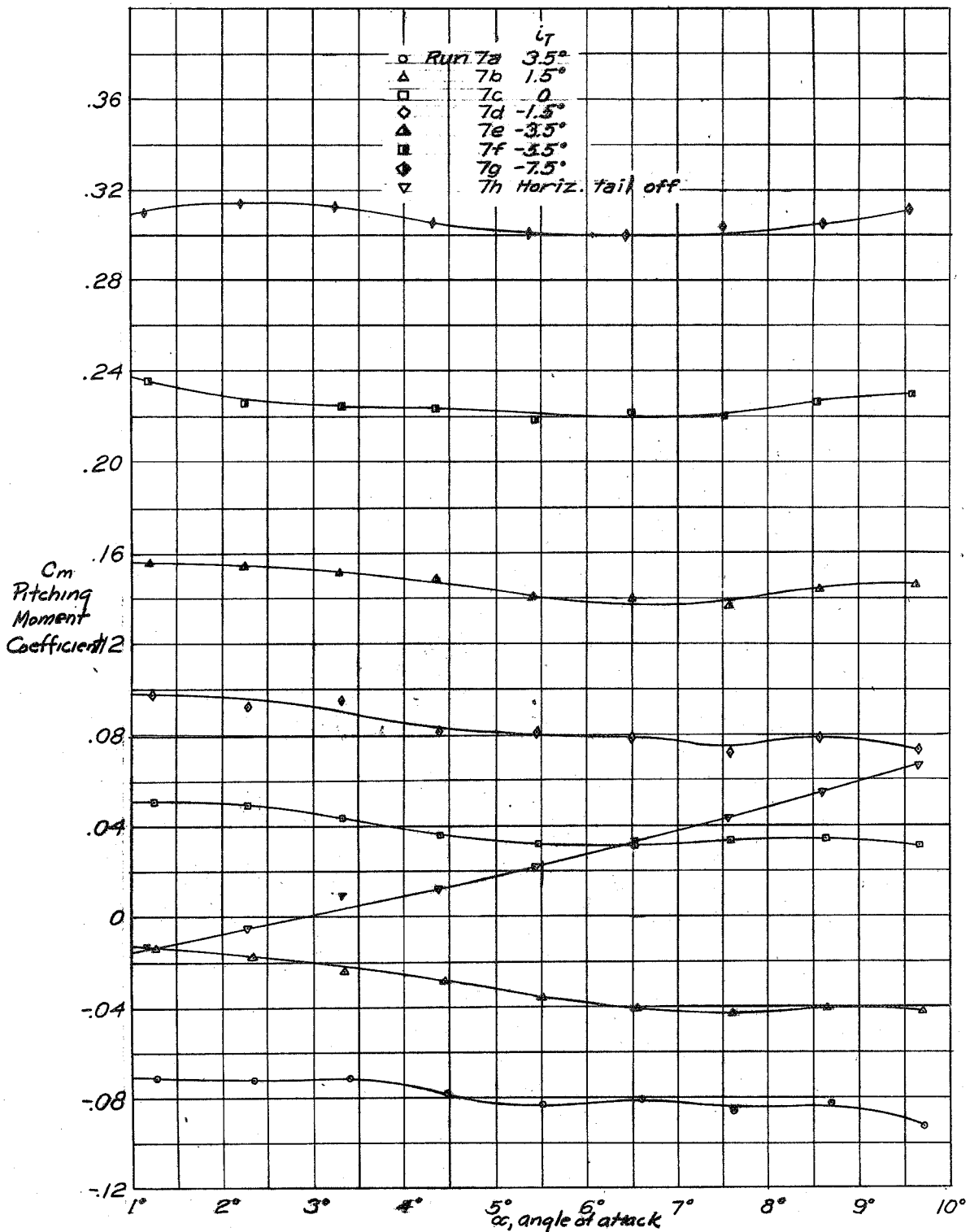

Fig. 11 (c). Effect of stabilizer setting on pitching moment. Both propellers rotating down toward the fuselage $\beta = 40.5°$
Rated power = 1625 horse power at 25,000 feet.

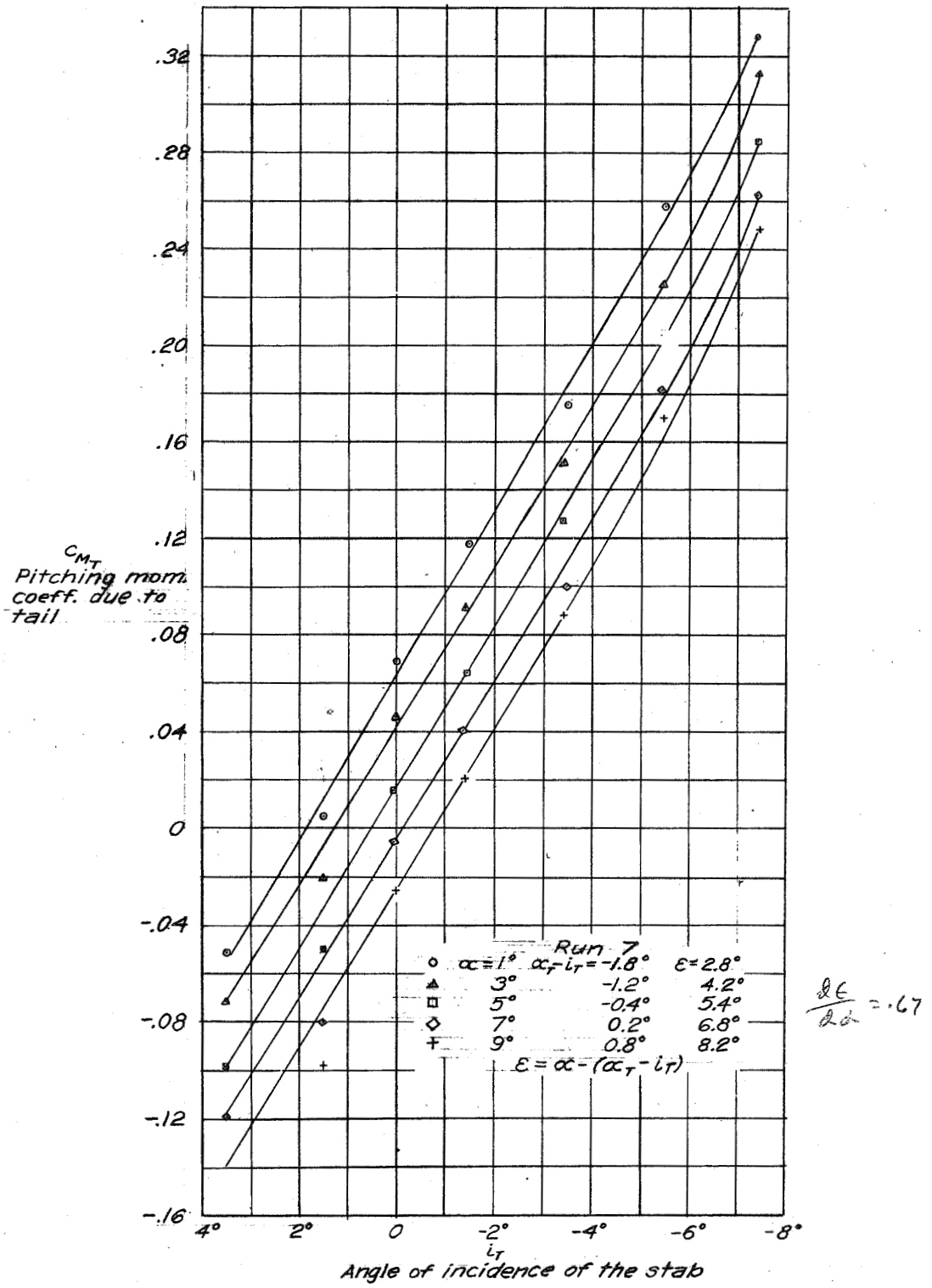

Fig. 11(d) Pitching moment of the horizontal tail surface vs. angle of incidence of the stabilizer. Both propellers rotating down toward the fuselage. $\beta = 40.5°$. Rated power = 1625 horsepower at 25,000 feet.

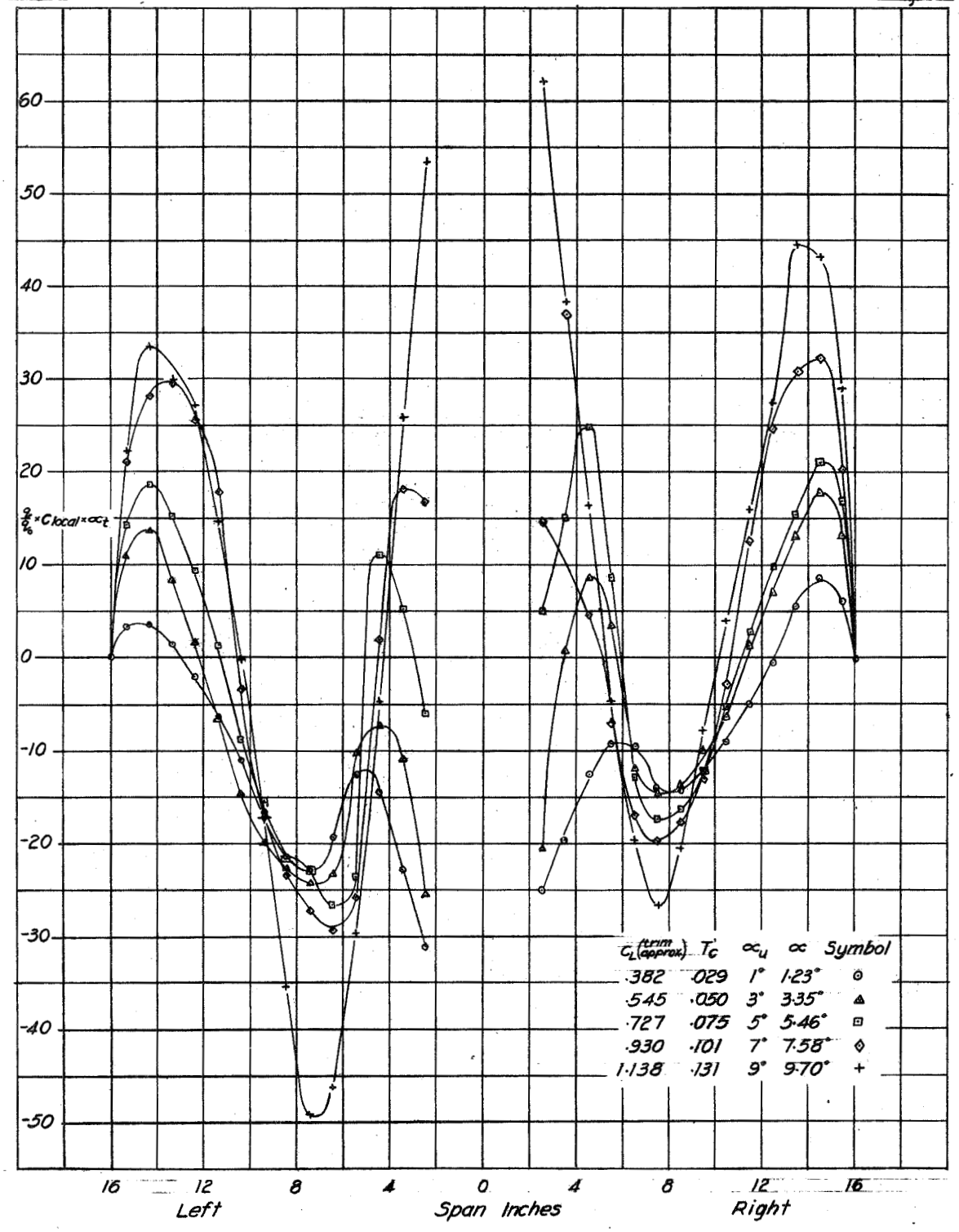

Fig. 11(e) Tail effectiveness factor. Variation of $q/q_0 \times C_{local} \times \alpha_t$ across horizontal tail span for $i_t = 1.5°$. Both propellers rotating down toward the fuselage. $\beta = 40.5°$. Rated power = 1625 horsepower at 25,000 feet.

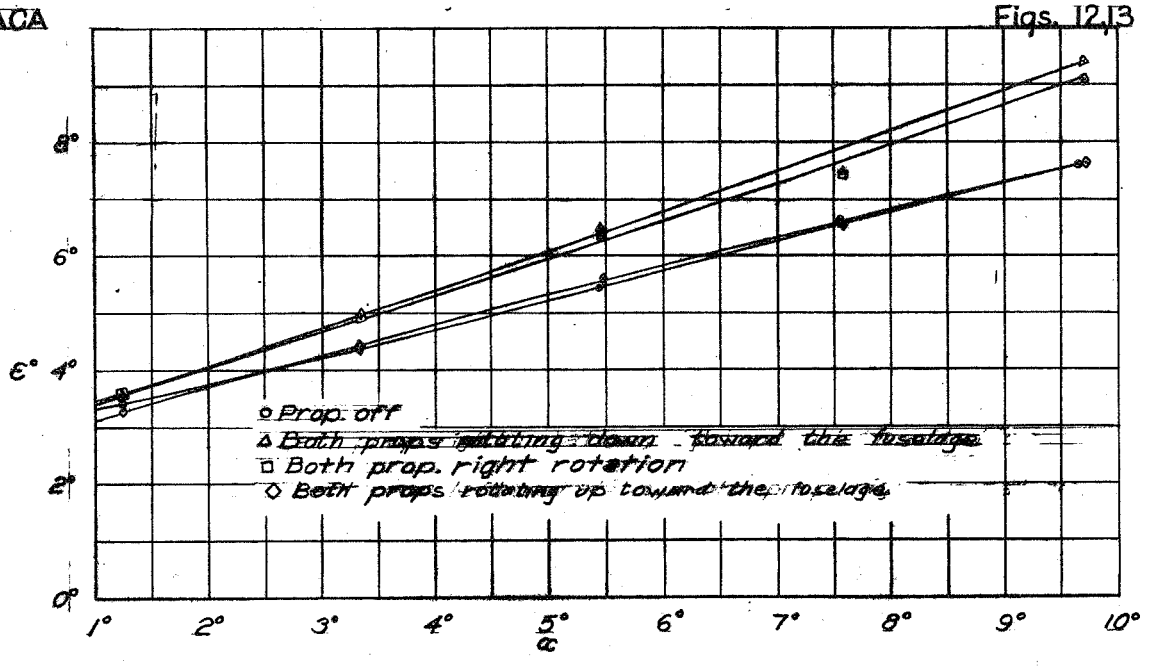

Fig. 12. Effect of propeller rotation on average downwash across horizontal tail span at approximately 25 percent chord line of horizontal tail from point by point survey. Rated power = 1625 horsepower at 25,000 feet, $\beta = 40.5°$

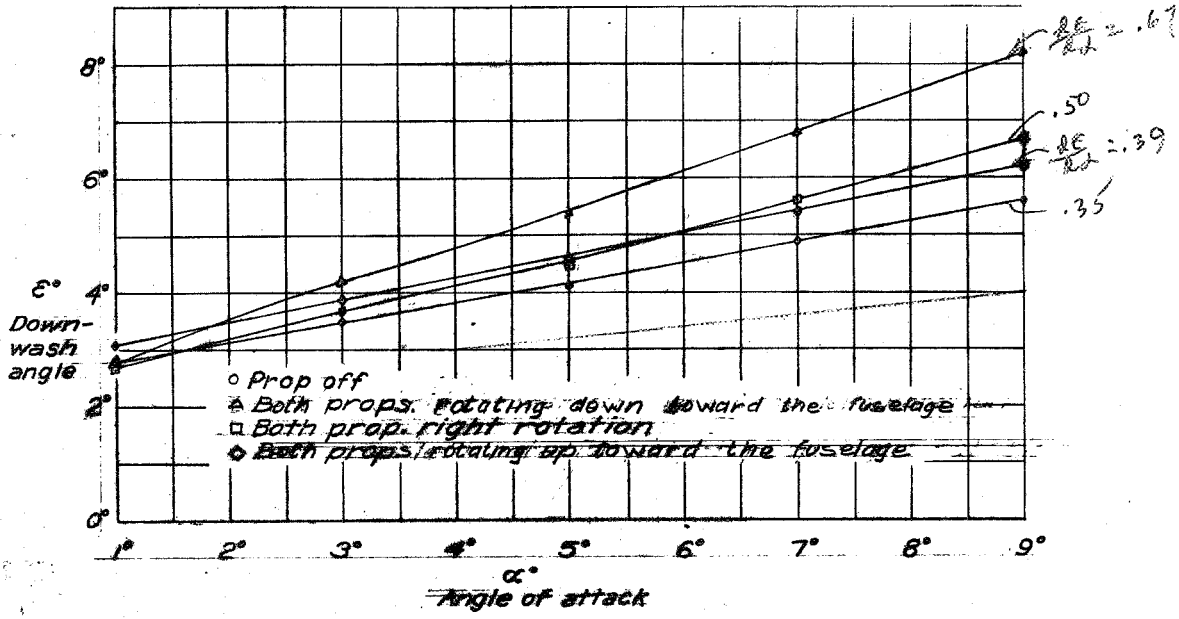

Fig. 13. Effect of propeller rotation on average downwash across horizontal tail span as obtained from angle of zero pitching moment of horizontal tail. Rated power = 1625 horsepower at 25,000 feet, $\beta = 40.5°$.

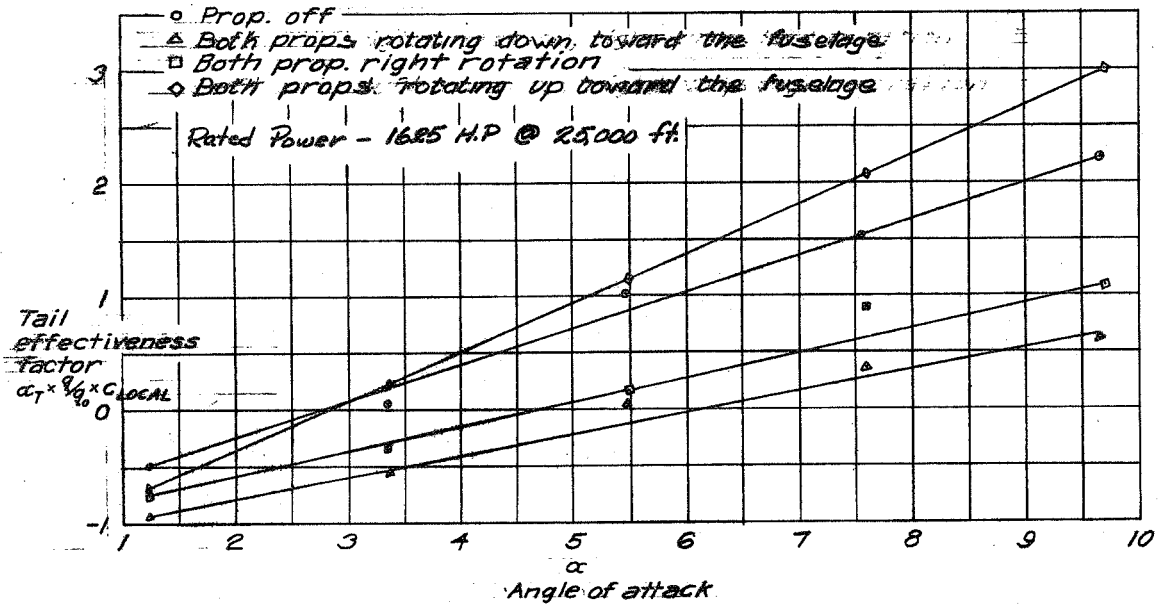

Fig. 14 Effect of propeller rotation on average tail effectiveness factor across horizontal tail span as obtained from point by point survey. Rated horse power at 25,000 feet = 1625 $\beta = 40.5°$.

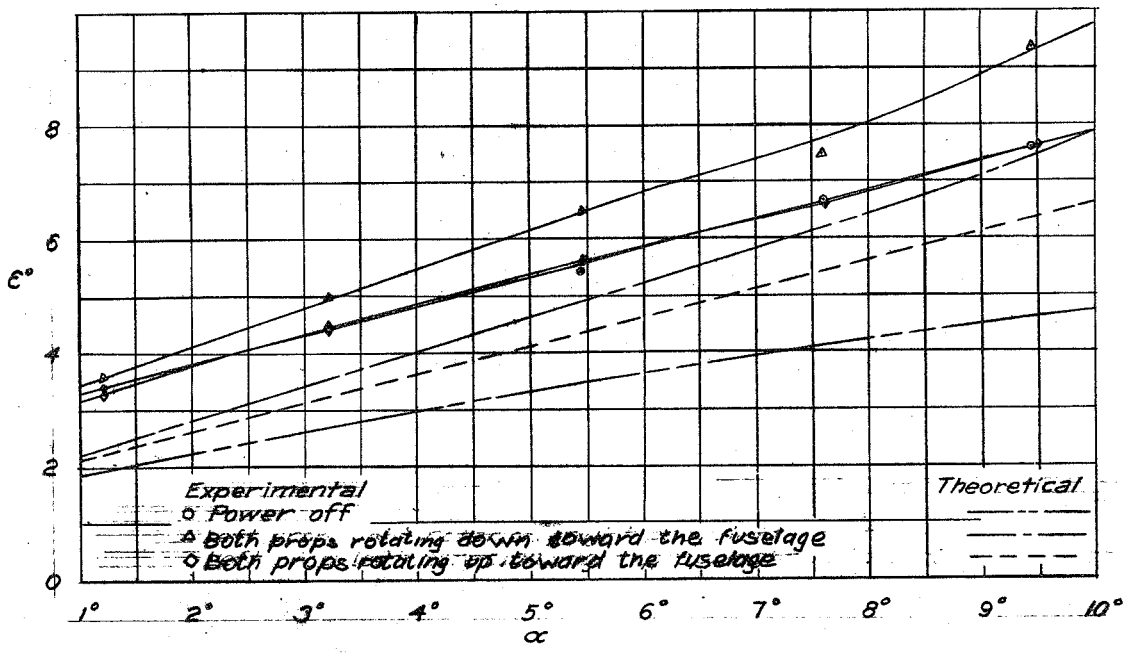

Fig. 19 Comparison of integrated theoretical downwash and the integrated downwash from the point by point surveys.

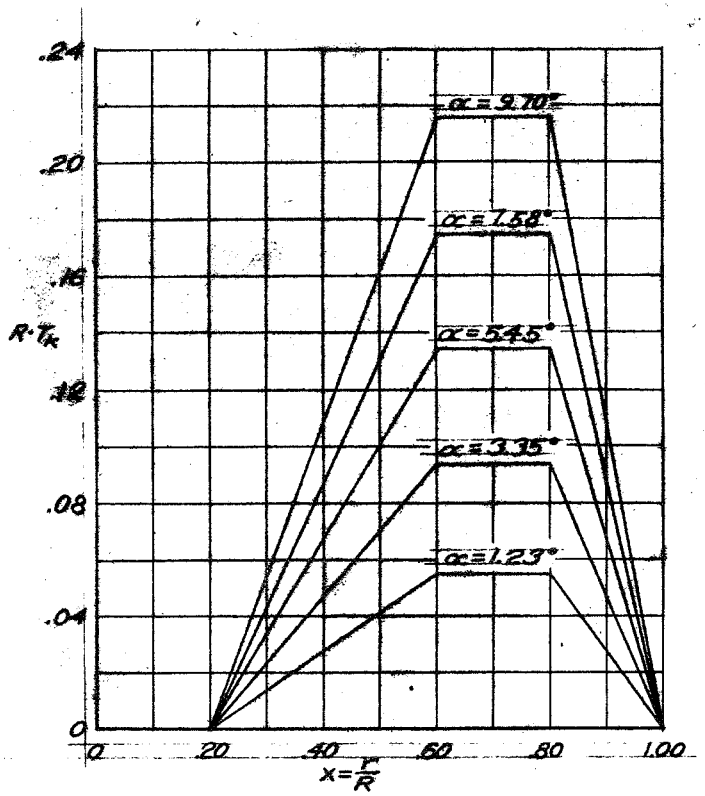

Fig 15 (b) Assumed thrust grading curves. Rated power = 1625 horsepower at 25,000 feet.

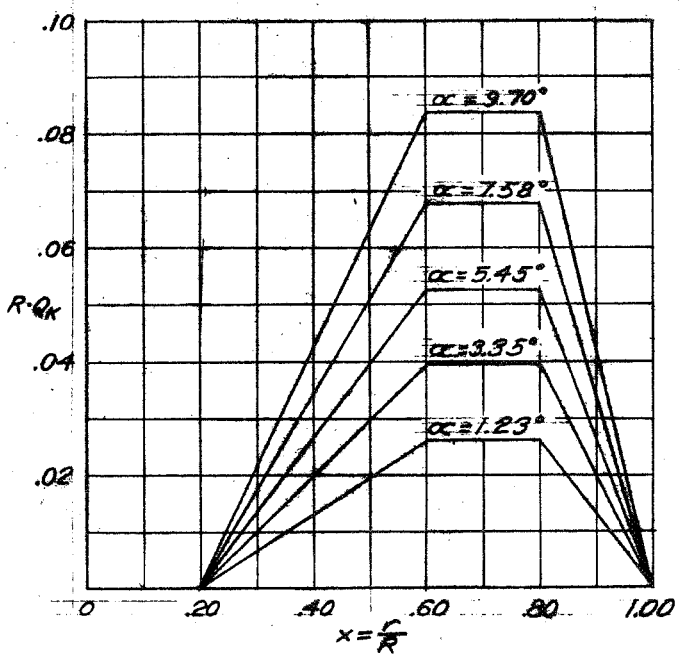

Fig 15 (a) Assumed torque grading curves. Rated power = 1625 horsepower at 25,000 feet, = 40.5°

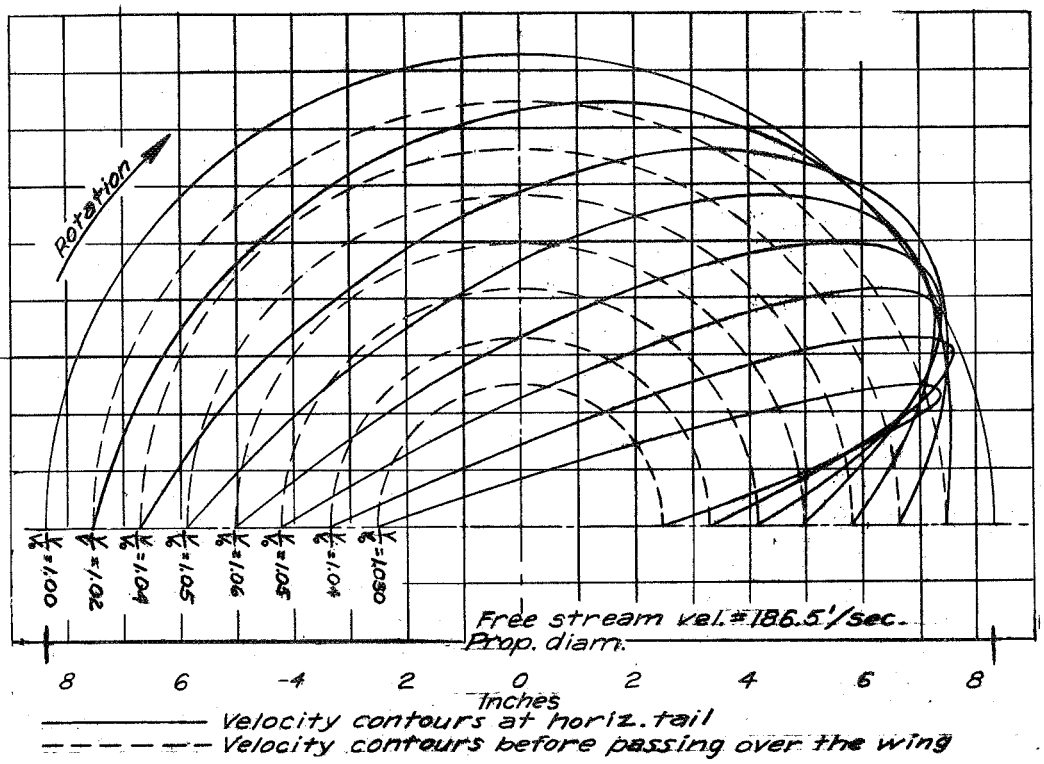

Fig. 16a Theoretical velocity contours in propeller wake just behind propeller and at horizontal tail. $\alpha = 9.7°$

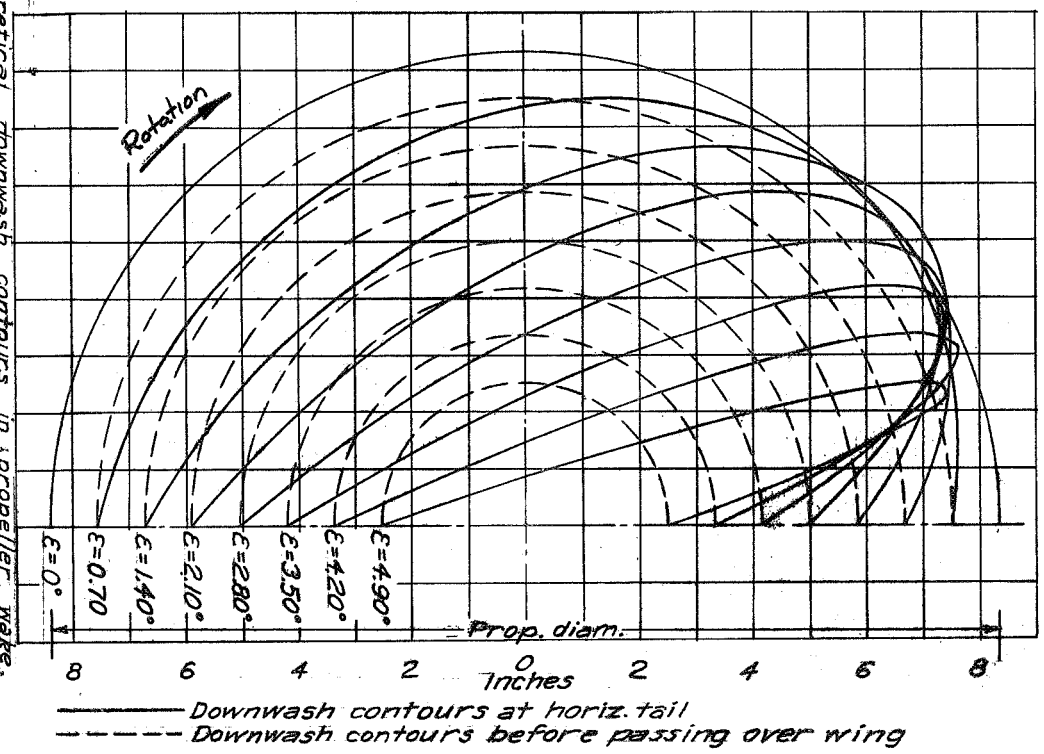

Fig. 16b Theoretical downwash contours in propeller wake, due to the propeller, just behind propeller and at horizontal tail $\alpha = 9.7°$

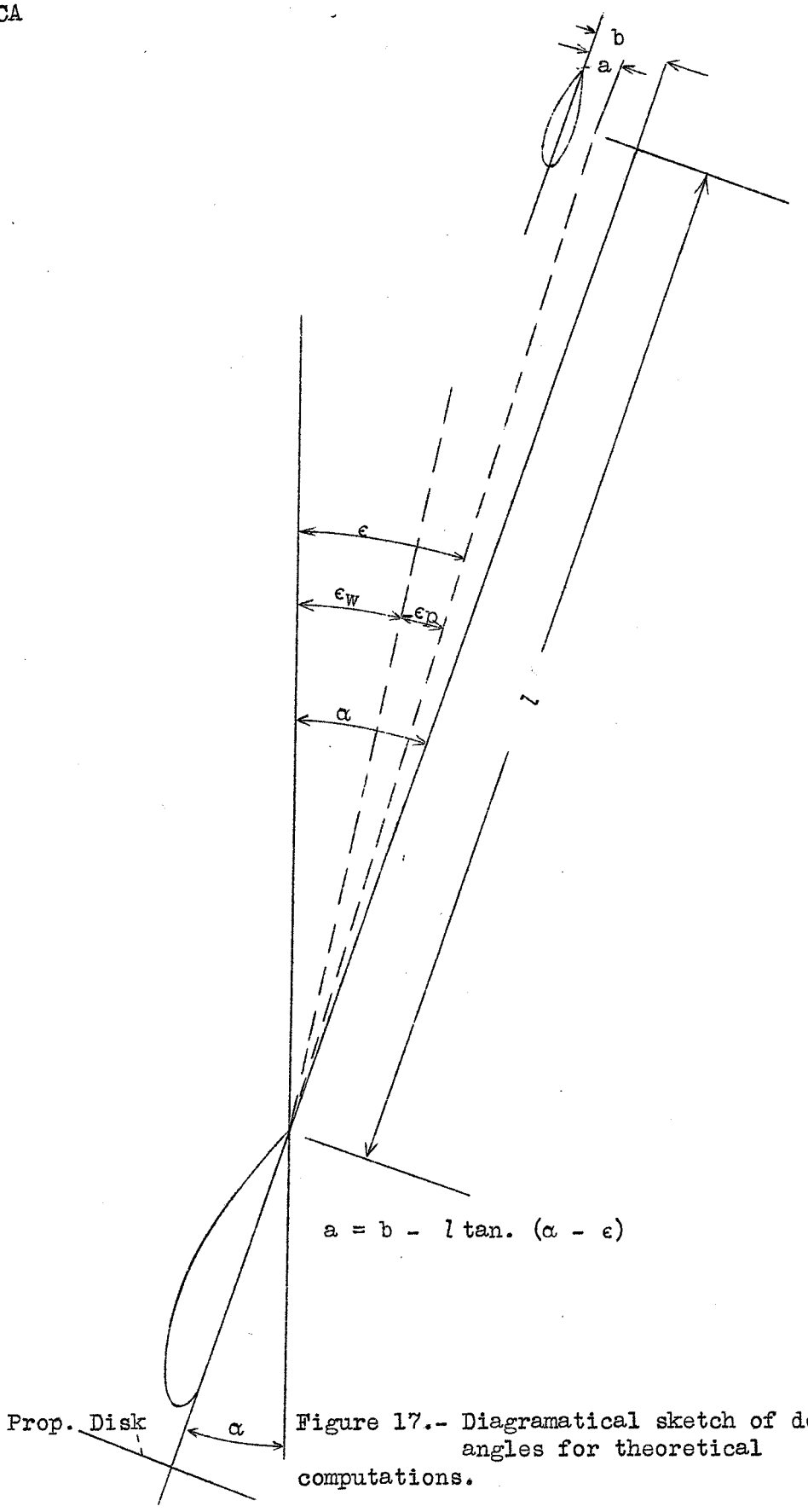

Figure 17.- Diagramatical sketch of downwash angles for theoretical computations.

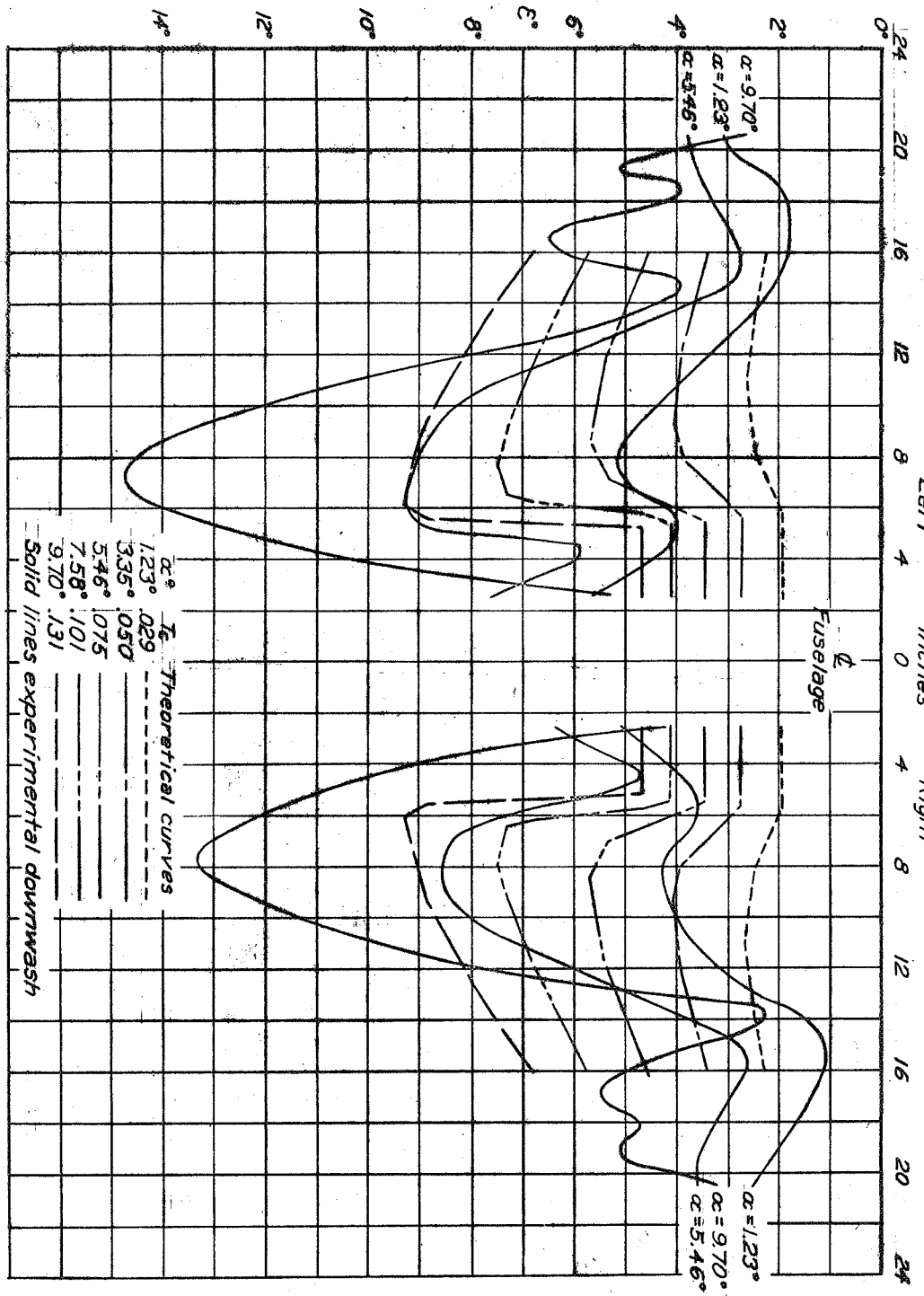

Fig. 18(a) Comparison of theoretical downwash across tail span with observed downwash. Both propellers rotating down toward the fuselage. $\beta = 40.5°$ Rated power = 1625 horse power at 25,000 feet.

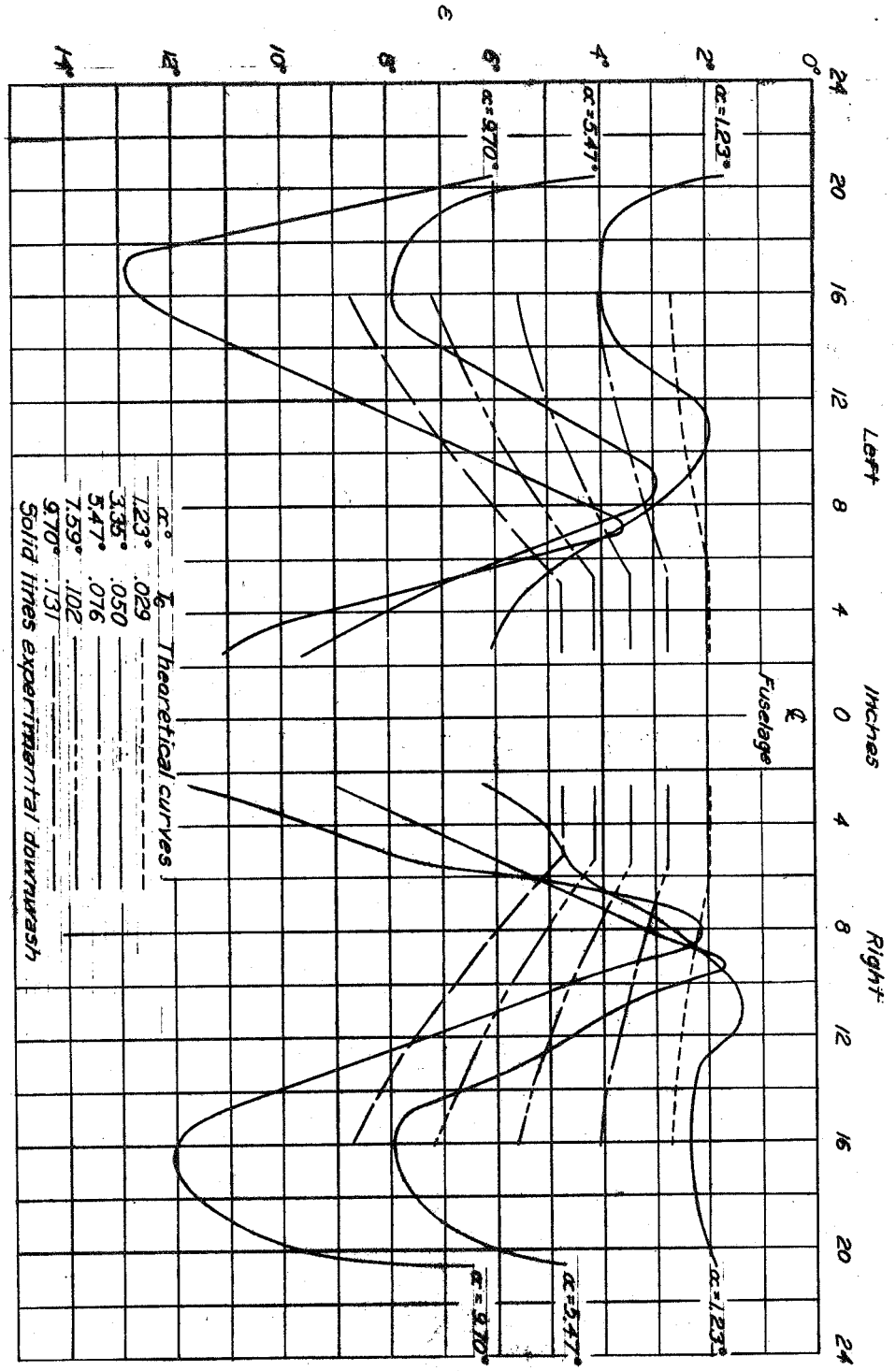

Fig. 18 (b) Comparison of theoretical downwash across tail span with observed downwash. Both propellers rotating up toward the fuselage. β = 40.5°. Rated power = 1625 horsepower at 25,000 feet.